

SEISMIC TESTS OF THE SUN'S INTERIOR STRUCTURE, COMPOSITION, AND AGE, AND IMPLICATIONS FOR SOLAR NEUTRINOS

D. B. GUENTHER

Department of Astronomy and Physics, Saint Mary's University, Halifax, NS, Canada, B3H 3C3

AND

P. DEMARQUE

Center for Solar and Space Research, Department of Astronomy, Yale University, New Haven, CT 06520-8101

Received 1996 October 28; accepted 1997 February 20

ABSTRACT

The structure of the deep interior of a variety of standard and nonstandard solar models constrained by the low- l p -mode oscillation data from GONG are presented. For standard models, we show that the effects of both helium and heavy-element diffusion must be included in order to find simultaneous agreement with both the p -mode spectrum and the observed value of $(Z/X)_{\odot}$. Related to this conclusion, we find that the average interior heavy-element abundance is greater than the observed surface abundance in models whose small spacings, which are derived from the p -mode oscillation spectra, best match the observations. The high-quality data from the Global Oscillation Network Group (GONG) now permit a precise determination of the seismic age of the Sun. The best agreement with the calculated oscillation spectra is achieved for 4.5 ± 0.1 Gyr, an age closely consistent with the age of the Sun inferred from meteorites, i.e., 4.53 ± 0.04 Gyr. This result lends strong support to the standard assumption of the theory of stellar evolution. With regard to the nonstandard solar models, we set limits on the extent to which the nonstandard assumptions can be applied to the model while still being consistent with the observed p -modes. The nonstandard assumptions investigated here are: forced mixing in the core, forced mixing in a shell surrounding the core, and near-zero heavy-element abundance in the core. These assumptions were selected because at one time or another they have all been proposed to reduce the neutrino flux of the solar model, thereby bringing the flux of the model more in line with the observed flux. All nonstandard models include helium and heavy element diffusion. We confirm, now using the latest solar model physics, that these nonstandard assumptions, when capable of reducing significantly the solar neutrino flux, perturb the interior structure too much to be consistent with p -mode observations. In addition, we set strict limits on the extent to which these nonstandard assumptions are tolerated by the current p -mode observations. For example, we show that the p -mode small spacings are incompatible with a low- Z core larger than $0.06 M_{\odot}$ in the Sun. And we show that if the Sun's core is chemically mixed, the extent of the mixed core cannot exceed $0.02 M_{\odot}$. The seismic data are also incompatible with extensive rapid mixing of ^4He in the solar envelope. This, we believe, also argues against the possibility of slow mixing of ^3He occurring in a shell, as was recently proposed by Cumming and Haxton to lower the $^7\text{Be}/^8\text{B}$ neutrino flux ratio. But we note that the occurrence of some mixing of ^3He and other trace elements and isotopes in the region of the solar interior where the initial ^4He abundance is nearly uniform (which could not at this point be detected by seismology) might modify the calculated neutrino fluxes.

Subject headings: nuclear reactions, nucleosynthesis, abundances — Sun: evolution — Sun: interior — Sun: oscillations

1. INTRODUCTION

1.1. Overview

The purpose of this paper is to explore the validity of some of the assumptions that affect the interior structure of the solar model using current solar p -mode data obtained from a network of telescopes. Using p -mode data from the Global Oscillation Network Group (GONG; Harvey et al. 1996), we have examined the importance of helium diffusion and Z diffusion, and we have tested the sensitivity of the model structure to the assumed initial heavy element content Z_{\odot} [or rather $(Z/X)_{\odot}$] and to the adopted age of the Sun. We have also explored three nonstandard assumptions which in the past have been proposed to explain the neutrino discrepancy: forced mixing in the core, forced mixing in a shell surrounding the core, and near-zero heavy-element abundance in the core. At the time these nonstandard assumptions were proposed, they could not be

easily ruled out by observation. But with the advent of helioseismology, they can be tested directly since the run of the speed of sound, probed by the p -mode oscillations, depends sensitively on the affected solar internal structure.

Individually or in combination, the eigenfunctions of the p -mode oscillations are sensitive to different regions in the Sun. Either by a full inversion of the oscillation equations of motion or by trial and error comparisons of systematically altered solar models, one can narrow in on an improved solar model, or test nonstandard solar models. Inverse methods produce a run of sound speed with error bars. The inverse method was used to locate the precise position of the base of the surface convection zone (Christensen-Dalsgaard, Gough & Thompson 1991), in essence, inferred from the location of a kink in the sound speed curve. Forward methods, where one calculates the oscillation spectrum of a model of the Sun and compares it to the

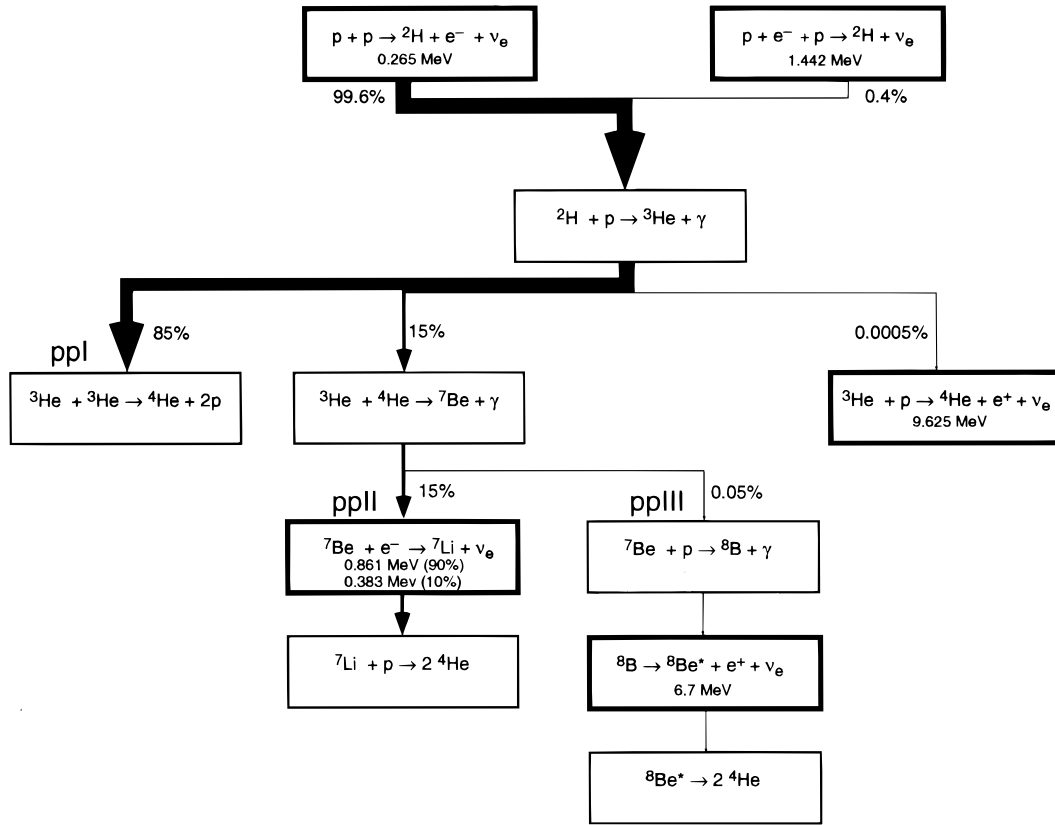


FIG. 1.—Flow chart for the *pp* reaction network with thick bordered boxes highlighting reactions that produce neutrinos. The termination probability (in percent) for each branch is shown for the standard solar model as is the average neutrino energy for the neutrino producing reactions.

observed spectrum and then alters some of the physics of the model, checking to see if the discrepancy between theory and observation is improved or worsened, have proven very effective in testing¹ the physical assumptions of the model. The forward approach was used to determine the sensitivity of the frequencies of the oscillation modes to the opacities, equation of state, age, composition, and surface boundary conditions of the model (Ulrich & Rhodes 1983; Guenther et al. 1992), and it was also used to test for the existence of helium diffusion (Cox, Guzik, & Kidman 1988).

In this work we will use the forward approach, as it is best suited to study the effect of modifications to the physical assumptions of the model on the *p*-mode frequencies, while still requiring our models to satisfy all the constraints of stellar structure (These constraints are not automatically satisfied in the inversion procedure). In the first half of this work we examine the current quality of the standard solar model. In the second half, we look at several examples of nonstandard solar model assumptions that can be tested using seismology. Because these particular nonstandard models were proposed as answers to the solar neutrino problem, we will also relate our results to the neutrino

observations. In the next two subsections we provide more background on the solar neutrino puzzle and solar seismology. In § 1.4 we provide a brief update on the meteoritic age determination of the Sun as this will later be compared to the seismological age.

1.2. Solar Neutrino Puzzle

The original solar neutrino problem pertained to the discrepancy between the observed neutrino flux and the significantly larger flux predicted by the standard solar model and the standard model of electroweak interactions. Today the problem also extends to reconciling the discrepant (within the context of the standard solar model) results of different neutrino experiments. For example, the data from the Kamiokande detector, which measures the flux of ⁸B neutrinos from the PP III reaction network (see chart of PP reaction network in Fig. 1) directly by real-time spectroscopy, are difficult to reconcile with the data from the radiochemical observatories, which provide data on the PP I and the PP II branches (Raghavan 1995). The oldest of the radiochemical observatories, the ³⁷Cl observatory in the Homestake mine (Davis 1993), detects mostly ⁸B neutrinos but is also sensitive to ⁷Be neutrinos, potentially yielding information about the relative importance of PP II and PP III in the Sun. The more recent ⁷¹Ga detectors of the GALLEX (Anselmann et al. 1994) and SAGE (Abdurashitov et al. 1994) observatories have complementary sensitivities to the PP I and PP II branches. The main puzzle is the basic incompatibility between the ratio of

¹ With the forward method it is not possible to definitively test whether or not an assumed process is occurring in the Sun. Other physical processes (not yet accounted for) may exist that perturb the oscillation frequencies in the opposite sense. Until we are confident that we have included all of the important physical processes, including magnetic fields, our tests are only conclusive within the set of physical processes so far studied.

$^7\text{Be}/^8\text{B}$ neutrino fluxes expected from nuclear and stellar interior physics and the observations. Hata et al. (1994) has argued that the problem goes beyond the standard nuclear/stellar physics framework of stellar energy generation. It also applies to the most popular nonstandard solar models proposed to explain the ^8B deficit because any known process that decreases the interior temperature, which decreases the ^7Be and ^8B neutrino fluxes, *increases* the ratio of these two fluxes, contrary to the observations. As a consequence, with the implication that the solution to the neutrino problem lies elsewhere, there is hope that solar neutrino science may lead to the discovery of the massive neutrino. From this perspective, testing new ideas in particle physics leading to the resolution of the solar neutrino anomalies depends on the availability of a robust and accurate model of the solar interior.

The degree to which the neutrino flux of the standard solar model can be adjusted by altering the model physics within the range of the known errors has been investigated thoroughly and carefully by many authors (Turck-Chièze et al. 1988; Sackmann, Boothroyd, & Fowler 1990; Bahcall & Pinsonneault 1992; several papers in Balantekin & Bahcall 1994; Chaboyer et al. 1995b). Their conclusions are similar: the physical parameters of the standard solar model cannot be adjusted in any manner, within the limits of the error bars, to lower the predicted neutrino flux enough to be consistent with the detected flux.

Furthermore, using the p -mode small spacings, which are sensitive to the regions closest to the center of the Sun, Elsworth et al. (1990) have shown that most standard solar models fit the p -mode observations very well. The question then naturally arises: does the standard solar model lack some important physical process that if included would result in a model with a lower flux of neutrinos? In other words, can the standard model be modified or improved in a reasonable way so as to reduce the predicted neutrino flux to a value consistent with neutrino flux measurements and at the same time be consistent with the p -mode observations?

When the neutrino problem first appeared, a large number of nonstandard solar model scenarios were invented to reduce the ^7Be and ^8B neutrino fluxes while keeping the total photon luminosity at its observed value (see, e.g., the reviews by Rood 1978; Bahcall 1989; Haxton 1995). In this work we will examine nonstandard solar models with low Z (abundance) cores and with mixed cores and shells. The nonstandard physics of these models directly alters the structure of the core and are testable to some extent using solar p -mode observations, as described in the next section. All of these nonstandard models, in some equivalent form, have been tested using p -mode frequencies before. Ulrich & Rhodes (1983) and Christensen-Dalsgaard & Gough (1980) were among the first to study the effect of nonstandard solar models on the p -modes, which at that time was done in part to improve the agreement between p -mode observations and solar model predictions. Many others have since carried out such comparisons (see recent review by Haxton 1995). The general conclusion from these earlier comparisons is that the p -mode observations are inconsistent with nonstandard models when the nonstandard physics is used to reduce the solar neutrino flux of the model enough to match the ^{37}Cl neutrino measurement.

In this work we examine some of these nonstandard models using the latest stellar structure physics, such as

diffusion and the OPAL equation of state tables that were not included during the earlier studies, and are known to affect the p -mode frequencies. The quality of the p -mode observations has improved significantly since these tests were made, and hence, we are now able to provide stronger constraints on the extent to which these nonstandard scenarios can be applied.

In the mixed core model some unspecified mechanism mixes the chemical elements in the core (Ezer & Cameron 1968). When the mixed core extends far enough outward, it dilutes the helium abundance in the central core burning region, which reduces the temperature, which, in turn, lowers the ^8B and ^7Be neutrino fluxes. Continuous mixing of a large fraction of the Sun is normally dismissed because if such mixing were to occur in other low-mass stars like the Sun, then the constant mixing of new hydrogen into the core would prevent the star from leaving the main sequence and evolving into a giant (Wheeler 1979). The mass in a fully mixed region near the center of other Sun-like stars can be constrained from observations of the color-magnitude diagram and luminosity function of open star clusters (Shaviv & Salpeter 1971; Prather & Demarque 1974; Demarque, Sarajedini, & Guo 1994; Dinescu et al. 1995). On the other hand, it can be argued that the sun is in a special phase of evolution when, for a short period, this mixing is taking place (Dilke & Gough 1972; Ezer & Cameron 1972; Rood 1972; Ulrich & Rood 1973).

In mixed envelope models the artificially mixed region is confined to an envelope that overlaps the nuclear burning core. By adjusting the location of the envelope one can control, to some extent, the relative importance of PP I, PP II, PP III, and CNO burning.

In the low- Z core model (Bahcall, Bahcall, & Ulrich 1968) the heavy-element abundance in a central region of the core is reduced. Reducing Z reduces the opacities which, in turn, reduces the temperature gradients needed to carry the required photon flux. As a consequence of the reduced temperature gradients the central temperature is reduced, and hence, so are the rates of neutrino production. Note that nonstandard solar models that reduce the interior opacity (Christensen-Dalsgaard 1992) mimic the features of the low- Z core model.

1.3. Seismology

The solar p -mode oscillations have already been used extensively to probe the interior of the Sun. To probe the deep interior, low- l p -modes are preferred because their inner turning points are located closest to the core (the low- l p -modes are still maximally sensitive to the outer layers were their eigenfunctions have the largest amplitudes but the relative contribution from deeper regions is greatest for the lowest l -values). In order to cancel out the sensitivity of the p -mode frequencies to the outer layers one can subtract from a given p -mode frequency the frequency of a p -mode with similar eigenfunction shape in the outer layers and distinct eigenfunction shape in the deeper layers. This can be achieved by forming the so called small spacing difference, defined as $\delta v(n, l) \equiv v(n, l) - v(n-1, l+2)$. This form is suggested by the asymptotic expression for frequency obtained by Tassoul (1980). She showed that in the limit of $n \gg l$ the frequency of a p -mode is given by

$$v(n, l) \approx \Delta v \left(n + \frac{1}{2} + \beta \right) + \frac{V_l \Delta v}{\pi v(n, l)}, \quad (1)$$

where the constants V'_l , Δv , and β depend on the structure, Δv is given by

$$\Delta v = \left(2 \int_0^R \frac{1}{c_s} dr \right)^{-1}, \quad (2)$$

where c_s is the sound speed and R is the radius. Because the largest contribution to Δv occurs near the surface where the sound speed c_s is smallest, we see that the first term on the right-hand side of equation (1) depends predominately on the structure near the surface. Using equation (1) to form the small spacing frequency difference $\nu(n, l) - \nu(n-1, l+2)$ one finds that the first term drops out, leaving

$$\nu(n, l) - \nu(n-1, l+2) \approx \frac{\Delta v}{\pi} \left(\frac{V'_l - V'_{l+2}}{\nu(n, l)} \right). \quad (3)$$

This can be expressed in terms of the sound speed as follows (see Tassoul 1980 for details):

$$\delta\nu(n, l) \approx -(4l+6) \frac{\Delta v}{4\pi^2\nu(n, l)} \int_0^R \frac{dc_s}{dr} \frac{dr}{r}. \quad (4)$$

We see that there is a significant contribution to $\delta\nu(n, l)$ from the integrand near the center of the Sun.

Until the recent availability of accurate low- l p -mode observations from GONG and the Birmingham Solar Oscillation Network (BiSON; Chaplin et al. 1996), we have not been able to use effectively the small spacings except as a gross indicator of the age of the model. In this work, though, we are able to show that the low- l data are accurate enough to constrain the age and interior Z of the model. In addition, the small spacing can be used to limit the extent of low- Z core and mixed core models.

Although the small spacing is the preferred diagnostic for the deep core because the p -mode frequencies are observed to such high accuracy (1 part in 10^4 to 1 part in 10^5) the p -mode frequencies can be used directly to test the interior structure of models. In addition, we note that because our test models have almost identical surface and atmospheric structures, all being based on a gray atmosphere with the Krishna Swamy empirical fit to the observed T - τ relation, the dominant surface layer sensitivity of the p -mode frequencies is nearly identical in all the models and can be ignored. We, therefore, also use the frequency difference plot (a plot of the model minus observed frequency versus observed frequency) to further explore the differences among the models and the Sun.

1.4. Meteoritic Age of the Sun

The age of the Sun is known from meteoritic dating (Guenther 1989, see also Christensen-Dalsgaard et al. 1996). The age of the Sun τ_\odot is defined as the time it has taken the Sun to evolve from the zero-age main sequence (ZAMS), where nuclear reactions just begin to dominate gravitation as the primary energy source, to the present day. Although it is common to simply set the age of the Sun equal to the age of the oldest meteorites, τ_m , properly, one should adjust for the fact that the oldest meteorites are older than the (ZAMS) Sun (Guenther 1989). The radioactive clocks of the meteorites are expected to be set to zero during the last high-temperature event in the primordial solar system nebula, which occurs before the Sun reaches the ZAMS. Observations of disks around T Tauri stars show that the

disk dissipates before the central star reaches the ZAMS. Based on pre-main-sequence evolution calculations and accounting for mass loss, Guenther (1989) has estimated the time between the zeroing of the meteoritic clocks and the ZAMS to be $\Delta\tau = 40 \pm 10$ Myr. The age of the Sun is then calculated from $\tau_\odot = \tau_m - \Delta\tau$. The error associated with the $\Delta\tau$ does not significantly affect the overall determination. Indeed, the time of formation of the meteorites, the time of the existence of the accretion disk, and the time of the emergence of the central star from the optically thick circumstellar cloud all occur within 10 Myr of each other (Strom, Edwards, & Skrutskie 1993). Bahcall, Pinsonneault, & Wasserburg 1995 estimate that the “solar system” age (which here corresponds to τ_m) to be between 4.563 and 4.576 Gyr. They did not attempt to relate this age, derived from a variety of meteoritic dating, to the evolutionary age of the Sun. Using their τ_m and Guenther’s $\Delta\tau$, we estimate the age of the Sun to be 4.53 ± 0.04 Gyr, which is the age we will adopt as the “meteoritic age” for the Sun.

2. METHOD

2.1. Solar Models

The Yale stellar evolution code (YREC for Yale Rotating Evolution Code) was used in its nonrotating configuration to construct the solar models (Guenther et al. 1992). YREC uses the nuclear energy generation routines of (Bahcall & Pinsonneault 1992) and the cross sections listed in Bahcall (1989). We have updated the cross section of the PP reaction, the ${}^7\text{Be}$ -proton capture reaction, and the hep reaction (Pinsonneault 1994, private communication). The equation of state tables prepared by the OPAL (Rogers 1986; Rogers, Swenson, & Iglesias 1996) researchers were used for the models.

Opacities in the interior were derived from the OPAL opacity tables (Iglesias & Rogers 1996), and opacities near the surface and the atmosphere were derived from the Alexander & Ferguson (1994) opacity tables. Z interpolation routines, which produce tables for a specified Z , are included with both sets of opacity tables. Because of the time-consuming nature of generating the tables for a given Z we calculated a set of Z specific tables at the beginning of each evolutionary run. To model Z diffusion and the low- Z core nonstandard solar models, where Z varies through the model, we generated two different Z specific tables at start-up, then carried out linear interpolation between the two tables to obtain opacity values at the Z value of each shell.

The effects of helium diffusion and heavy-element diffusion are included in some of the models. The diffusion formulation is identical to that described by Bahcall et al. (1995). We note that the heavy-element diffusion coefficients and equations are for iron alone. We have assumed, for this calculation, that the iron diffusion rate, scaled to the total Z mass abundance, is equal to the total Z diffusion rate. This assumption is certainly not correct, but at this time we cannot carry out more sophisticated calculations.

The effects of rotation are not included in any of the model calculations presented here. As discussed in detail in Chaboyer et al. (1995a, 1995b) rotation tends to inhibit the effects of diffusion by approximately a factor of 2.

All models were evolved from a zero-age main sequence (ZAMS) model to near the age of the Sun in 50 equally spaced time steps. By adjusting the helium abundance and mixing length parameter of each model, the models were

tuned to have identical radii to one part in 10^7 ($R_\odot = 6.958 \times 10^{10}$ cm) and identical luminosities ($L_\odot = 3.8515 \times 10^{33}$ ergs s^{-1}) to one part in 10^6 . To obtain numerically accurate (± 1 μ Hz) p -mode frequencies from the models (using our first-order pulsation code), it is necessary to use approximately 1800 shells divided equally among the interior (inner 95% of the model), the envelope (outer 5% of the model), and the atmosphere (from the photosphere outward to the temperature minimum). The atmosphere is modeled using the Krishna Swamy (1966) T - τ relation. This relation is derived from a fit to the Sun's observed T - τ dependence in the lower atmosphere.

The run of the Z in the initial ZAMS model was modified to produce the low- Z solar models. The metal abundance was set to $Z_i = 1.0 \times 10^{-6}$ from the center outward toward mass fraction q_i at which point the metal abundance was linearly increased to Z_{surf} over the mass fraction interval q_i to $q_0 \equiv q_i + 0.025$. From mass fraction q_0 outward the metal abundance was kept constant. Both nuclear burning and heavy-element diffusion alter the initial Z profile as the model is evolved. YREC linearly interpolates between two distinct Z opacity tables to obtain the opacity at the Z for a given shell. Low- Z solar models were constructed for low- Z core sizes $q_i = 0.020$ – 0.200 .

The mixed-core and envelope models were constructed by artificially forcing a mixing event, i.e., a homogenization of the chemical elements, in the core of the model after each evolutionary time step. Mixed-core models were constructed for mixed-core sizes q (the extent of the mixed core in mass fraction) = 0.05 – 0.4 . The mixing process in the mixed-core models was not conceived to correspond to any known physical process. It is entirely artificial. If mixing does occur in the core of the Sun, it is unlikely the mass extent of the mixed core is constant throughout the evolutionary history of the Sun. The mixed-core models presented here should only be considered as extremely crude approximations of any physical core mixing processes.

The physical characteristics of the standard solar models are summarized in Table 1, and the physical characteristics of the nonstandard solar models, the mixed core models and the low- Z core models are summarized in Table 2. From left to right, Tables 1 and 2 list: Model, the model number; Diffusion (Table 1 only), the type of diffusion included in the model, where Y stands for helium diffusion only and Y & Z stands for helium and metal diffusion; Age (Table 1 only), the age of the model in Gyr; Mixing (Table 2 only), the region of the model near the core that is mixed, in mass fraction; q_i (Table 2 only), the extent of the low- Z core in mass fraction; X_{init} , the initial or ZAMS mass fraction value of hydrogen; Z_{init} , the initial or ZAMS mass fraction value of all heavy elements; X_{surf} , the surface mass fraction of hydrogen at the evolved age; Z_{surf} , the surface mass fraction of all heavy elements at the evolved age; M_{env} , the fraction of the total mass contained in the outer convective envelope; R_{env} , the radius fraction of the base of the convective envelope; $\log P_c$, the base ten logarithm of the central pressure; $\log T_c$, the base 10 logarithm of the central temperature; $\log \rho_c$, the base 10 logarithm of the central density; X_c , the central mass fraction of hydrogen; Z_c , the central mass fraction of heavy elements; $\Phi(^{37}\text{Cl})$, the total neutrino flux, in SNU, for the ^{37}Cl detector; and $\Phi(^{71}\text{Ga})$, the total neutrino flux, in SNU, for the ^{71}Ga detector. Tables 3 and 4 list some of the nuclear energy generation properties of the standard and nonstandard solar models.

Specifically they list the fraction of the total photon luminosity coming from the PP I, PP II, and PP III branches of the PP network and from the CNO cycle; and they list the individual neutrino fluxes from the neutrino producing reactions that occur in the sun (see Fig. 1).

2.2. p -Mode Frequencies

Oscillation frequencies of the models were calculated using Guenther's nonradial, nonadiabatic pulsation program (Guenther 1994) for a selected set of modes with l ranging from 0 to 100. Only radiative nonadiabatic effects in the Eddington approximation are accounted for. To compare with observations we used data from GONG (specifically the merged multi-month averaged data set, mrvnx951120v1, which contains averaged data from 1995 August 23 to 1996 February 18).

We found the traditional approach of plotting the small spacings of the models and the Sun opposite the observed frequencies to be unsatisfactory. To compare the small spacings of the models to each other and to the observations we instead plotted small spacing differences [i.e., $\delta_{\text{model}}(n, l) - \delta_\odot(n, l)$] as a function of the corresponding observed frequency $\nu_\odot(n, l)$. In these plots, of course, the closer $\delta_{\text{model}}(n, l) - \delta_\odot(n, l)$ is to 0 μ Hz the better, although we will assume there is agreement between the observations and a model when the data points lie within the bounds of the plotted error bars. Error bars were calculated as the sum of the errors of the two observed modes used to calculate the observed small spacing differences.

Small spacings are presented for $l = 0, 1, 2, 3, 5$, and 10 . The sensitivity of the small spacings to the core regions diminishes with increasing l . There is little resolvable sensitivity to the core regions in the small spacings for $l \geq 5$.

In frequency difference plots (model frequency minus observed frequency versus observed frequency), the primary component of the discrepancy, visible as an increase in discrepancy with increasing frequency, is a consequence of the errors in the structure of the superadiabatic layer and atmosphere of the model (Demarque, Guenther, & Kim 1997). Modifications to the superadiabatic layer structure alone can remove the *slope* discrepancy. The remaining discrepancy identified with the spread of the data points at a given frequency (i.e., the thickness of the bundle of lines) is associated with small errors in the structure of the interior model. For the frequency difference plots, we judge the quality of the agreement by how tightly together the bundle of lines joining common l -values are and ignore the underlying slope error, knowing it to be due almost exclusively to modeling errors in the outermost layers.

We note that as the frequency of the p -modes increase so do their sensitivity to perturbations to the structure (see, e.g., Christensen-Dalsgaard 1986). This is a direct consequence of the fact that the integrated kinetic energy of an oscillation mode (often called the mode mass or mode inertia) decreases rapidly with increasing frequency and less rapidly with increasing l . In fact, it can be shown (Christensen-Dalsgaard 1986) that to first order the perturbation to the frequency by a perturbation to the structure is inversely proportional to the mode mass. As a consequence, small structural changes lead to correspondingly larger frequency perturbations at higher frequencies and at higher l -values than they do at lower frequencies and lower l -values. To facilitate comparisons of the frequency perturbations of different l -values, at *similar frequencies*, one can

TABLE 1
STANDARD SOLAR MODEL CHARACTERISTICS

Model	Diffusion	Age	X_{init}	Z_{init}	X_{surf}	Z_{surf}	M_{env}	R_{env}	$\log P_c$	$\log T_c$	$\log \rho_c$	X_c	Z_c	$\Phi(^{37}\text{Cl})$	$\Phi(^{71}\text{Ga})$
1.....	none	4.5	0.7237	0.0170	0.7237	0.0170	0.0184	0.7320	17.364	7.188	2.171	0.374	0.0170	5.80	120
2.....	none	4.5	0.7033	0.0200	0.7033	0.0200	0.0210	0.7240	17.366	7.194	2.177	0.351	0.0200	7.52	129
3.....	none	4.5	0.6892	0.0230	0.6892	0.0230	0.0227	0.7190	17.367	7.199	2.181	0.334	0.0230	9.06	137
4.....	none	4.7	0.7257	0.0170	0.7257	0.0170	0.0191	0.7300	17.369	7.189	2.179	0.364	0.0170	6.06	121
5.....	none	4.7	0.7052	0.0200	0.7052	0.0200	0.0220	0.7210	17.372	7.195	2.186	0.341	0.0200	7.85	131
6.....	none	4.7	0.6911	0.0230	0.6911	0.0230	0.0236	0.7160	17.372	7.200	2.190	0.324	0.0230	9.45	139
7.....	none	4.9	0.7277	0.0170	0.7277	0.0170	0.0198	0.7280	17.374	7.190	2.188	0.354	0.0170	6.33	123
8.....	none	4.9	0.7072	0.0200	0.7072	0.0200	0.0226	0.7200	17.377	7.197	2.195	0.331	0.0200	8.19	132
9.....	none	4.9	0.6931	0.0230	0.6931	0.0230	0.0242	0.7150	17.378	7.202	2.199	0.314	0.0230	9.85	141
10.....	Y	4.5	0.7248	0.0170	0.7420	0.0170	0.0204	0.7240	17.367	7.189	2.175	0.369	0.0170	6.04	121
11.....	Y	4.5	0.7044	0.0200	0.7215	0.0200	0.0232	0.7160	17.370	7.195	2.182	0.346	0.0200	7.85	131
12.....	Y	4.5	0.6904	0.0230	0.7075	0.0230	0.0250	0.7110	17.370	7.200	2.186	0.329	0.0230	9.47	139
13.....	Y	4.7	0.7268	0.0170	0.7442	0.0170	0.0210	0.7220	17.373	7.190	2.184	0.359	0.0170	6.32	123
14.....	Y	4.7	0.7064	0.0200	0.7238	0.0200	0.0241	0.7130	17.376	7.197	2.191	0.336	0.0200	8.20	132
15.....	Y	4.7	0.6924	0.0230	0.7098	0.0230	0.0257	0.7090	17.376	7.202	2.195	0.318	0.0230	9.89	141
16.....	Y	4.9	0.7288	0.0170	0.7465	0.0170	0.0218	0.7200	17.378	7.191	2.193	0.349	0.0170	6.60	124
17.....	Y	4.9	0.7084	0.0200	0.7261	0.0200	0.0251	0.7110	17.381	7.198	2.200	0.326	0.0200	8.57	134
18.....	Y	4.9	0.6944	0.0230	0.7121	0.0230	0.0269	0.7060	17.382	7.203	2.204	0.308	0.0230	10.30	143
19.....	Y&Z	4.5	0.7261	0.0170	0.7575	0.0152	0.0203	0.7250	17.369	7.190	2.178	0.363	0.0179	6.37	123
20.....	Y&Z	4.5	0.7059	0.0200	0.7378	0.0180	0.0234	0.7160	17.372	7.197	2.185	0.339	0.0211	8.35	133
21.....	Y&Z	4.5	0.6917	0.0230	0.7240	0.0208	0.0259	0.7080	17.373	7.203	2.190	0.320	0.0242	10.10	142
22.....	Y&Z	4.7	0.7282	0.0170	0.7600	0.0152	0.0213	0.7220	17.375	7.191	2.187	0.352	0.0179	6.68	124
23.....	Y&Z	4.7	0.7079	0.0200	0.7403	0.0180	0.0242	0.7140	17.377	7.199	2.194	0.328	0.0211	8.74	135
24.....	Y&Z	4.7	0.6937	0.0230	0.7265	0.0207	0.0265	0.7070	17.378	7.204	2.199	0.310	0.0243	10.60	145
25.....	Y&Z	4.9	0.7302	0.0170	0.7624	0.0152	0.0221	0.7190	17.380	7.193	2.196	0.342	0.0180	7.00	126
26.....	Y&Z	4.9	0.7100	0.0200	0.7428	0.0179	0.0250	0.7120	17.383	7.200	2.203	0.318	0.0211	9.15	137
27.....	Y&Z	4.9	0.6958	0.0230	0.7291	0.0207	0.0275	0.7050	17.384	7.205	2.208	0.299	0.0243	11.10	147

multiply each frequency difference (model frequency minus observed frequency) by the corresponding mode mass and divide by the mode mass of a radial mode at the same frequency (Q_{nl}). This eliminates the l dependence of the frequency perturbation. This weighting is important when considering a wide range of l -values (e.g., $0 \leq l \leq 2000$) but

is much less important for the range of l -values considered here ($0 \leq l \leq 100$), as can be seen by comparing the plots in to the plots in Figure 2a with mode mass weighting to Figure 2b without mode mass weighting. Because the weighting does not significantly alter the basic features of the diagrams we use unweighted frequency differences.

TABLE 2
NONSTANDARD SOLAR MODEL CHARACTERISTICS

Model	Mixing ^a	q_i^a	X_{init}	Z_{init}	X_{surf}	Z_{surf}	M_{env}^a	R_{env}	$\log P_c$	$\log T_c$	$\log \rho_c$	X_c	Z_c	$\Phi(^{37}\text{Cl})$	$\Phi(^{71}\text{Ga})$
28.....	0.00–0.01	none	0.7079	0.200	0.7403	0.0180	0.0241	0.7140	17.374	7.201	2.169	0.373	0.0210	9.08	136
29.....	0.00–0.02	none	0.7077	0.200	0.7401	0.0180	0.0241	0.7140	17.370	7.202	2.154	0.394	0.0210	9.71	138
30.....	0.00–0.04	none	0.7072	0.200	0.7397	0.0180	0.0240	0.7150	17.361	7.202	2.132	0.425	0.0209	11.00	142
31.....	0.00–0.06	none	0.7065	0.200	0.7392	0.0180	0.0243	0.7130	17.351	7.202	2.112	0.450	0.0209	12.00	145
32.....	0.00–0.08	none	0.7058	0.200	0.7386	0.0180	0.0238	0.7150	17.342	7.201	2.096	0.469	0.0208	12.50	146
33.....	0.00–0.10	none	0.7049	0.200	0.7381	0.0180	0.0239	0.7150	17.332	7.200	2.080	0.486	0.0208	12.70	146
34.....	0.00–0.15	none	0.7029	0.200	0.7366	0.0179	0.0231	0.7170	17.311	7.197	2.050	0.518	0.0207	12.20	143
35.....	0.00–0.20	none	0.7009	0.200	0.7354	0.0179	0.0223	0.7190	17.295	7.194	2.027	0.541	0.0206	11.20	139
36.....	0.00–0.30	none	0.6976	0.200	0.7336	0.0178	0.0207	0.7230	17.270	7.189	1.995	0.574	0.0205	9.17	130
37.....	0.00–0.40	none	0.6949	0.200	0.7326	0.0177	0.0187	0.7290	17.252	7.185	1.973	0.597	0.0204	7.54	123
38.....	0.00–0.50	none	0.6930	0.200	0.7323	0.0177	0.0172	0.7330	17.241	7.182	1.960	0.612	0.0204	6.50	118
39.....	0.05–0.10	none	0.7077	0.200	0.7401	0.0180	0.0240	0.7140	17.375	7.198	2.192	0.329	0.0211	8.67	135
40.....	0.05–0.20	none	0.7055	0.200	0.7387	0.0179	0.0233	0.7160	17.360	7.194	2.178	0.336	0.0211	7.95	131
41.....	0.05–0.30	none	0.7028	0.200	0.7372	0.0179	0.0219	0.7190	17.346	7.190	2.164	0.344	0.0211	6.95	126
42.....	0.10–0.15	none	0.7078	0.200	0.7403	0.0180	0.0242	0.7140	17.376	7.198	2.193	0.329	0.0211	8.66	135
43.....	0.10–0.20	none	0.7074	0.200	0.7401	0.0180	0.0241	0.7140	17.374	7.197	2.191	0.330	0.0211	8.42	134
44.....	0.10–0.30	none	0.7060	0.200	0.7393	0.0179	0.0232	0.7160	17.368	7.195	2.186	0.334	0.0211	7.73	130
45.....	0.20–0.25	none	0.7079	0.200	0.7403	0.0180	0.0241	0.7140	17.377	7.199	2.194	0.328	0.0211	8.72	135
46.....	0.20–0.30	none	0.7078	0.200	0.7402	0.0180	0.0240	0.7150	17.377	7.198	2.194	0.329	0.0211	8.65	135
47.....	0.20–0.40	none	0.7072	0.200	0.7400	0.0180	0.0236	0.7150	17.376	7.198	2.193	0.329	0.0211	8.48	134
48.....	none	0.02	0.7084	0.200	0.7419	0.0179	0.0213	0.7260	17.375	7.183	2.189	0.369	0.0001	7.00	128
49.....	none	0.04	0.7089	0.200	0.7423	0.0179	0.0216	0.7240	17.378	7.177	2.193	0.378	0.0001	5.76	123
50.....	none	0.06	0.7098	0.200	0.7429	0.0179	0.0215	0.7250	17.382	7.173	2.199	0.383	0.0001	4.87	119
51.....	none	0.08	0.7109	0.200	0.7437	0.0179	0.0218	0.7240	17.387	7.170	2.205	0.386	0.0001	4.25	116
52.....	none	0.10	0.7121	0.200	0.7446	0.0180	0.0222	0.7230	17.393	7.169	2.212	0.387	0.0001	3.83	113
53.....	none	0.15	0.7159	0.200	0.7472	0.0180	0.0232	0.7200	17.406	7.167	2.227	0.386	0.0001	3.28	110
54.....	none	0.20	0.7205	0.200	0.7503	0.0181	0.0250	0.7150	17.418	7.168	2.241	0.381	0.0001	3.13	108

^a Mass fraction.

TABLE 3
STANDARD SOLAR MODEL NUCLEAR DATA

MODEL	FRACTION OF TOTAL LUMINOSITY				SOLAR NEUTRINO FLUX							
	PP I	PP II	PP III	CNO	PP	PeP	HeP	⁷ Be	⁸ B	¹³ N	¹⁵ O	¹⁷ F
1.....	0.8940	0.0901	0.0076	0.0089	6.07E+00	1.45E-2	1.29E-7	4.09E-1	3.97E-4	3.41E-2	2.78E-2	3.29E-4
2.....	0.8750	0.1030	0.0087	0.0132	5.99E+00	1.41E-2	1.23E-7	4.69E-1	5.31E-4	4.96E-2	4.23E-2	5.08E-4
3.....	0.8600	0.1130	0.0095	0.0181	5.91E+00	1.37E-2	1.19E-7	5.13E-1	6.51E-4	6.68E-2	5.85E-2	7.09E-4
4.....	0.8910	0.0927	0.0078	0.0093	6.06E+00	1.45E-2	1.29E-7	4.21E-1	4.18E-4	3.52E-2	2.91E-2	3.44E-4
5.....	0.8720	0.1060	0.0089	0.0138	5.97E+00	1.41E-2	1.23E-7	4.82E-1	5.57E-4	5.14E-2	4.42E-2	5.32E-4
6.....	0.8560	0.1160	0.0098	0.0188	5.89E+00	1.37E-2	1.19E-7	5.27E-1	6.81E-4	6.93E-2	6.12E-2	7.43E-4
7.....	0.8870	0.0954	0.0080	0.0096	6.04E+00	1.45E-2	1.29E-7	4.33E-1	4.38E-4	3.63E-2	3.04E-2	3.61E-4
8.....	0.8680	0.1090	0.0092	0.0144	5.95E+00	1.41E-2	1.22E-7	4.95E-1	5.84E-4	5.32E-2	4.63E-2	5.58E-4
9.....	0.8520	0.1190	0.0100	0.0197	5.87E+00	1.37E-2	1.18E-7	5.41E-1	7.13E-4	7.20E-2	6.41E-2	7.79E-4
10.....	0.8910	0.0923	0.0078	0.0092	6.06E+00	1.45E-2	1.29E-7	4.19E-1	4.16E-4	3.52E-2	2.89E-2	3.43E-4
11.....	0.8720	0.1060	0.0089	0.0138	5.97E+00	1.41E-2	1.23E-7	4.80E-1	5.57E-4	5.14E-2	4.41E-2	5.31E-4
12.....	0.8560	0.1160	0.0098	0.0188	5.89E+00	1.37E-2	1.18E-7	5.26E-1	6.83E-4	6.95E-2	6.11E-2	7.44E-4
13.....	0.8880	0.0951	0.0080	0.0096	6.05E+00	1.45E-2	1.28E-7	4.32E-1	4.38E-4	3.64E-2	3.03E-2	3.60E-4
14.....	0.8680	0.1090	0.0092	0.0144	5.95E+00	1.41E-2	1.22E-7	4.94E-1	5.85E-4	5.34E-2	4.62E-2	5.58E-4
15.....	0.8520	0.1190	0.0100	0.0197	5.87E+00	1.37E-2	1.18E-7	5.41E-1	7.16E-4	7.23E-2	6.41E-2	7.81E-4
16.....	0.8840	0.0979	0.0083	0.0100	6.03E+00	1.45E-2	1.28E-7	4.44E-1	4.60E-4	3.77E-2	3.17E-2	3.78E-4
17.....	0.8640	0.1120	0.0094	0.0150	5.94E+00	1.41E-2	1.22E-7	5.08E-1	6.14E-4	5.54E-2	4.84E-2	5.86E-4
18.....	0.8480	0.1220	0.0103	0.0206	5.85E+00	1.37E-2	1.17E-7	5.55E-1	7.50E-4	7.52E-2	6.73E-2	8.20E-4
19.....	0.8870	0.0948	0.0080	0.0101	6.04E+00	1.45E-2	1.28E-7	4.30E-1	4.42E-4	3.82E-2	3.18E-2	3.79E-4
20.....	0.8670	0.1090	0.0092	0.0152	5.95E+00	1.40E-2	1.22E-7	4.94E-1	5.96E-4	5.64E-2	4.89E-2	5.92E-4
21.....	0.8500	0.1190	0.0101	0.0209	5.86E+00	1.36E-2	1.17E-7	5.42E-1	7.34E-4	7.67E-2	6.82E-2	8.34E-4
22.....	0.8840	0.0977	0.0082	0.0105	6.03E+00	1.45E-2	1.28E-7	4.44E-1	4.66E-4	3.97E-2	3.34E-2	4.00E-4
23.....	0.8630	0.1120	0.0095	0.0159	5.93E+00	1.40E-2	1.21E-7	5.09E-1	6.28E-4	5.88E-2	5.15E-2	6.25E-4
24.....	0.8460	0.1230	0.0104	0.0220	5.84E+00	1.36E-2	1.17E-7	5.58E-1	7.71E-4	8.03E-2	7.19E-2	8.81E-4
25.....	0.8800	0.1010	0.0085	0.0110	6.01E+00	1.45E-2	1.27E-7	4.57E-1	4.91E-4	4.13E-2	3.51E-2	4.21E-4
26.....	0.8590	0.1150	0.0097	0.0167	5.91E+00	1.40E-2	1.21E-7	5.23E-1	6.60E-4	6.14E-2	5.42E-2	6.59E-4
27.....	0.8410	0.1260	0.0106	0.0231	5.82E+00	1.36E-2	1.16E-7	5.73E-1	8.09E-4	8.40E-2	7.59E-2	9.30E-4

3. STANDARD SOLAR MODELS

3.1. Overview of the Models

As we are primarily concerned with the core of the Sun, we have examined those physical parameters that affect the

core most. Within the context of the standard solar model, they are the age and the composition. The composition is itself affected by nuclear processes, convection, and diffusion. We assume the nuclear processes are already well enough established and, within the context of the standard

TABLE 4
NONSTANDARD SOLAR MODEL NUCLEAR DATA

MODEL	FRACTION OF TOTAL LUMINOSITY				SOLAR NEUTRINO FLUX							
	PP I	PP II	PP III	CNO	PP	PeP	HeP	⁷ Be	⁸ B	¹³ N	¹⁵ O	¹⁷ F
28.....	0.8620	0.1130	0.0095	0.0162	5.92E+00	1.40E-2	1.21E-7	5.12E-1	6.57E-4	5.98E-2	5.25E-2	6.40E-4
29.....	0.8600	0.1140	0.0096	0.0167	5.92E+00	1.39E-2	1.21E-7	5.17E-1	7.12E-4	6.13E-2	5.40E-2	6.65E-4
30.....	0.8570	0.1160	0.0098	0.0173	5.90E+00	1.39E-2	1.20E-7	5.28E-1	8.27E-4	6.35E-2	5.63E-2	7.05E-4
31.....	0.8550	0.1180	0.0100	0.0175	5.89E+00	1.38E-2	1.18E-7	5.36E-1	9.15E-4	6.42E-2	5.70E-2	7.23E-4
32.....	0.8550	0.1180	0.0100	0.0174	5.89E+00	1.37E-2	1.16E-7	5.38E-1	9.62E-4	6.37E-2	5.66E-2	7.21E-4
33.....	0.8550	0.1180	0.0100	0.0170	5.90E+00	1.36E-2	1.14E-7	5.37E-1	9.81E-4	6.25E-2	5.54E-2	7.07E-4
34.....	0.8610	0.1140	0.0097	0.0157	5.92E+00	1.35E-2	1.08E-7	5.21E-1	9.44E-4	5.79E-2	5.08E-2	6.47E-4
35.....	0.8680	0.1090	0.0093	0.0141	5.96E+00	1.33E-2	1.03E-7	4.96E-1	8.61E-4	5.22E-2	4.60E-2	5.80E-4
36.....	0.8830	0.0979	0.0083	0.0111	6.03E+00	1.31E-2	9.35E-8	4.44E-1	6.93E-4	3.89E-2	3.78E-2	4.69E-4
37.....	0.8960	0.0878	0.0074	0.0092	6.09E+00	1.29E-2	8.64E-8	3.98E-1	5.60E-4	3.18E-2	3.18E-2	3.88E-4
38.....	0.9050	0.0806	0.0068	0.0081	6.13E+00	1.28E-2	8.21E-8	3.66E-1	4.75E-4	2.78E-2	2.79E-2	3.36E-4
39.....	0.8640	0.1110	0.0094	0.0158	5.93E+00	1.40E-2	1.21E-7	5.07E-1	6.22E-4	5.83E-2	5.10E-2	6.18E-4
40.....	0.8700	0.1080	0.0091	0.0142	5.96E+00	1.38E-2	1.15E-7	4.88E-1	5.64E-4	5.26E-2	4.62E-2	5.56E-4
41.....	0.8790	0.1010	0.0085	0.0120	6.00E+00	1.36E-2	1.06E-7	4.60E-1	4.84E-4	4.27E-2	4.02E-2	4.78E-4
42.....	0.8640	0.1110	0.0094	0.0158	5.93E+00	1.40E-2	1.21E-7	5.07E-1	6.20E-4	5.83E-2	5.10E-2	6.18E-4
43.....	0.8660	0.1100	0.0093	0.0152	5.94E+00	1.40E-2	1.20E-7	5.01E-1	6.01E-4	5.60E-2	4.96E-2	6.00E-4
44.....	0.8710	0.1060	0.0090	0.0136	5.97E+00	1.39E-2	1.14E-7	4.81E-1	5.45E-4	4.82E-2	4.55E-2	5.48E-4
45.....	0.8630	0.1120	0.0094	0.0159	5.93E+00	1.40E-2	1.21E-7	5.08E-1	6.25E-4	5.89E-2	5.13E-2	6.23E-4
46.....	0.8640	0.1110	0.0094	0.0161	5.93E+00	1.40E-2	1.20E-7	5.06E-1	6.19E-4	6.01E-2	5.09E-2	6.17E-4
47.....	0.8650	0.1100	0.0093	0.0160	5.93E+00	1.40E-2	1.17E-7	5.02E-1	6.06E-4	6.21E-2	4.99E-2	6.04E-4
48.....	0.8730	0.1060	0.0089	0.0129	5.97E+00	1.42E-2	1.23E-7	4.81E-1	4.82E-4	4.85E-2	4.10E-2	4.90E-4
49.....	0.8810	0.0996	0.0084	0.0113	6.01E+00	1.45E-2	1.24E-7	4.52E-1	3.78E-4	4.28E-2	3.54E-2	4.13E-4
50.....	0.8890	0.0936	0.0079	0.0097	6.05E+00	1.47E-2	1.26E-7	4.25E-1	3.06E-4	3.76E-2	3.01E-2	3.44E-4
51.....	0.8960	0.0884	0.0074	0.0085	6.08E+00	1.50E-2	1.27E-7	4.01E-1	2.58E-4	3.34E-2	2.59E-2	2.91E-4
52.....	0.9020	0.0840	0.0071	0.0077	6.10E+00	1.52E-2	1.29E-7	3.81E-1	2.25E-4	3.04E-2	2.30E-2	2.55E-4
53.....	0.9110	0.0766	0.0064	0.0064	6.14E+00	1.58E-2	1.32E-7	3.47E-1	1.85E-4	2.59E-2	1.87E-2	2.05E-4
54.....	0.9150	0.0729	0.0061	0.0064	6.16E+00	1.64E-2	1.35E-7	3.30E-1	1.74E-4	2.67E-2	1.73E-2	1.91E-4

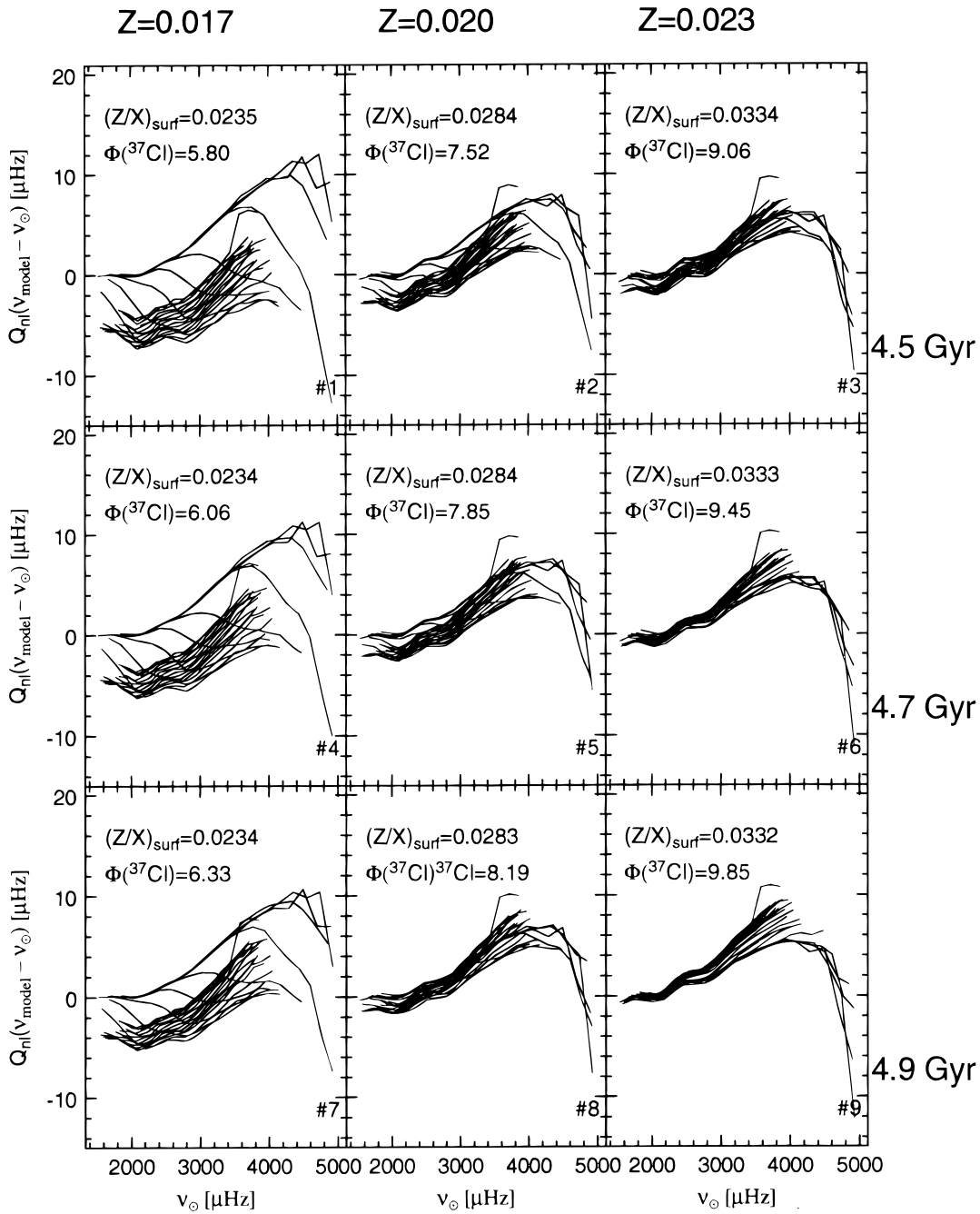


FIG. 2a

FIG. 2.—(a) Grid of plots, each showing the p -mode frequency differences, model minus Sun, weighted by the normalized mode mass Q_{nl} (Christensen-Dalsgaard 1986) for models that do not include diffusion. Each plot is annotated with the surface Z/X ratio and the ^{37}Cl neutrino flux, in SNU. The model number (see Table 1) is also indicated. The observational data are from GONG. The weighted frequency differences more accurately represent the relative sensitivities of the mode differences to structural differences. The effect though is not significant for the lower l -values plotted here. See discussion in text. (b) The p -mode frequency differences data in (a) not weighted. As in (a), each plot is annotated with the surface Z/X ratio and the ^{37}Cl neutrino flux, in SNU. The model number (see Table 1) is also indicated.

solar model, are not a source of significant uncertainty in the determination of the structure of the core. In the standard solar model, convection does not play a role in the core.

For models without diffusion, with helium diffusion, and with helium and heavy element diffusion (see models 1–27 in Table 1 and 3), we constructed 3×3 grids spanning Z_{init}

and age. Age was set to one of the following: 4.5, 4.7, and 4.9 Gyr, while Z_{init} was set to one of the following: 0.017, 0.020, and 0.023.

3.2. Helium Abundance

Referring to Table 1, we note that the range of values in

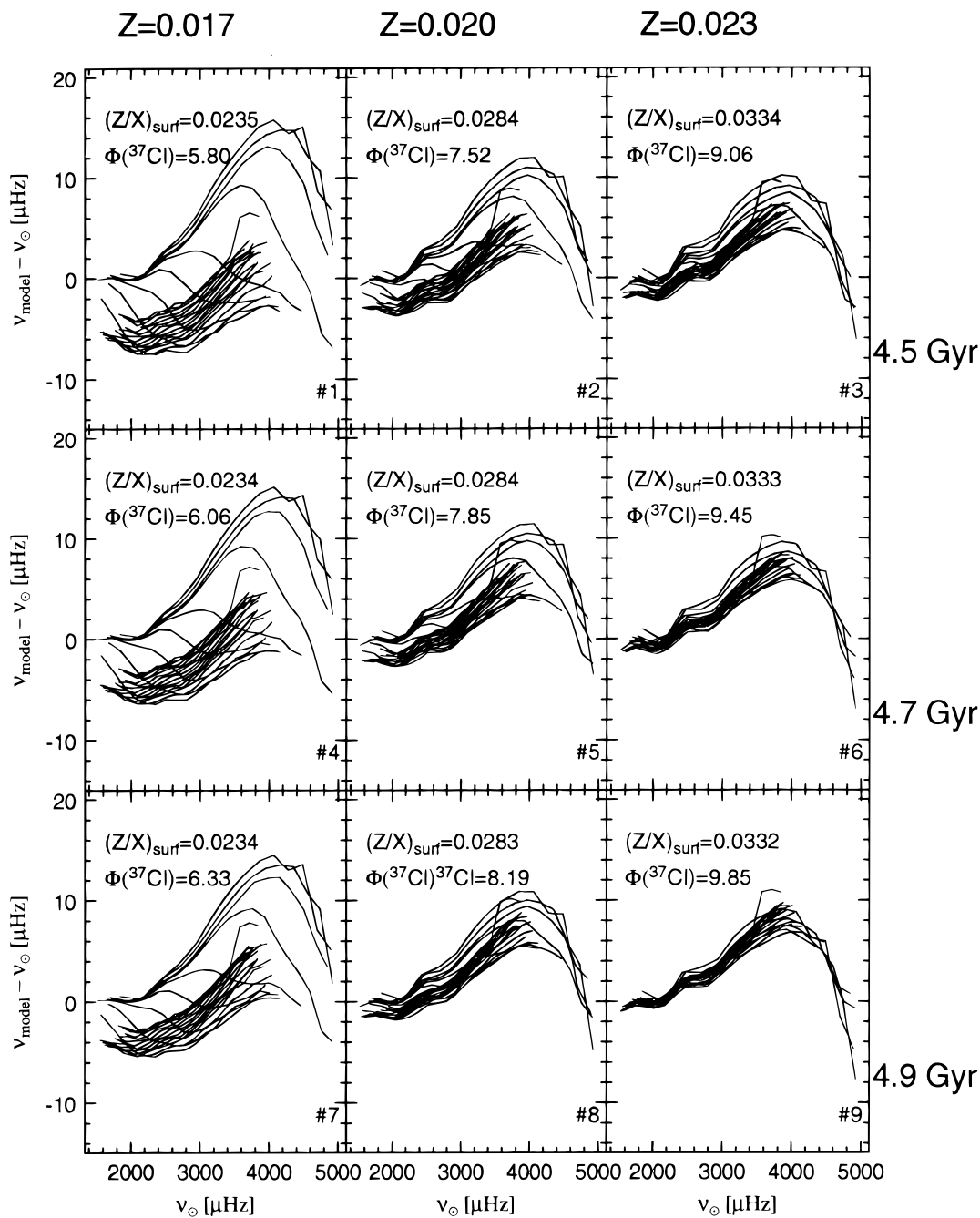


FIG. 2b

X_{surf} is greater than the range of values in X_{init} . Although helioseismology is able to determine X_{surf} , currently the best way to determine the initial hydrogen and helium abundance remains direct modeling of the Sun. This is due not only to the lower sensitivity of X_{init} to basic solar model physics, such as diffusion (Chaboyer et al. 1995b), when compared to X_{surf} , but also the high sensitivity of the luminosity of the model to the central helium abundance: the luminosity of a lower main-sequence star goes as $\mu^{7.5}$, where μ is the mean molecular weight. Furthermore, helioseismology is relatively insensitive to the helium abundance below the convection zone because hydrogen and helium are fully ionized in the deep interior, and the ratio of specific heats γ , upon which the sound speed depends, is nearly

constant and equal to 5/3 for all compositions. The situation is more hopeful near the surface, in the hydrogen and helium ionization zones, where γ is variable and leaves a stronger signature on the run of the sound speed. Recent determinations of the helium abundance by inversion yield results that are encouragingly consistent with solar models and the conclusion that helium diffusion has taken place in the solar convection zone (Däppen & Gough 1986; Antia & Basu 1994). Regardless, it is important to astronomers to know both X_{surf} and X_{init} — X_{surf} is used to validate models of helium diffusion and X_{init} is used as a key datum in the study of the Galaxy's chemical evolution, which in turn helps constrain the nuclear evolution of the universe. Our best standard solar model will establish both values.

3.3. Neutrino Flux

The neutrino flux of the standard solar model increases with Z_{init} and with age (see Table 1). This is because the central temperature of the models is directly correlated to the central helium mass fraction. And the central helium mass fraction of the models increases with increasing Z_{init} and with increasing age. The models with the lowest Z_{init} and age, which have the lowest central helium abundance, have the lowest neutrino fluxes. For the standard solar models listed in Table 1, the neutrino flux for ^{37}Cl detectors does not fall below 5.8 SNU (model 1). The neutrino flux at a specific solar age increases when helium diffusion is included in the model, and increases again, when heavy-element diffusion is also included in the model. Both helium

diffusion and heavy-element diffusion lead to slightly greater central helium abundances. These results are consistent with the results of Bahcall et al. (1995).

3.4. Helioseismology

3.4.1. Overview

Turning to the seismic properties of the models, we show in Figures 2b, 3, and 4 frequency difference plots (model minus observed) for models 1–9 (no diffusion), 10–18 (Y diffusion only), and 19–27 (Y and Z diffusion). Each figure contains nine individual plots laid out in a 3×3 grid corresponding to the different values of age, running vertically, and Z_{init} , running horizontally. Annotating each plot are

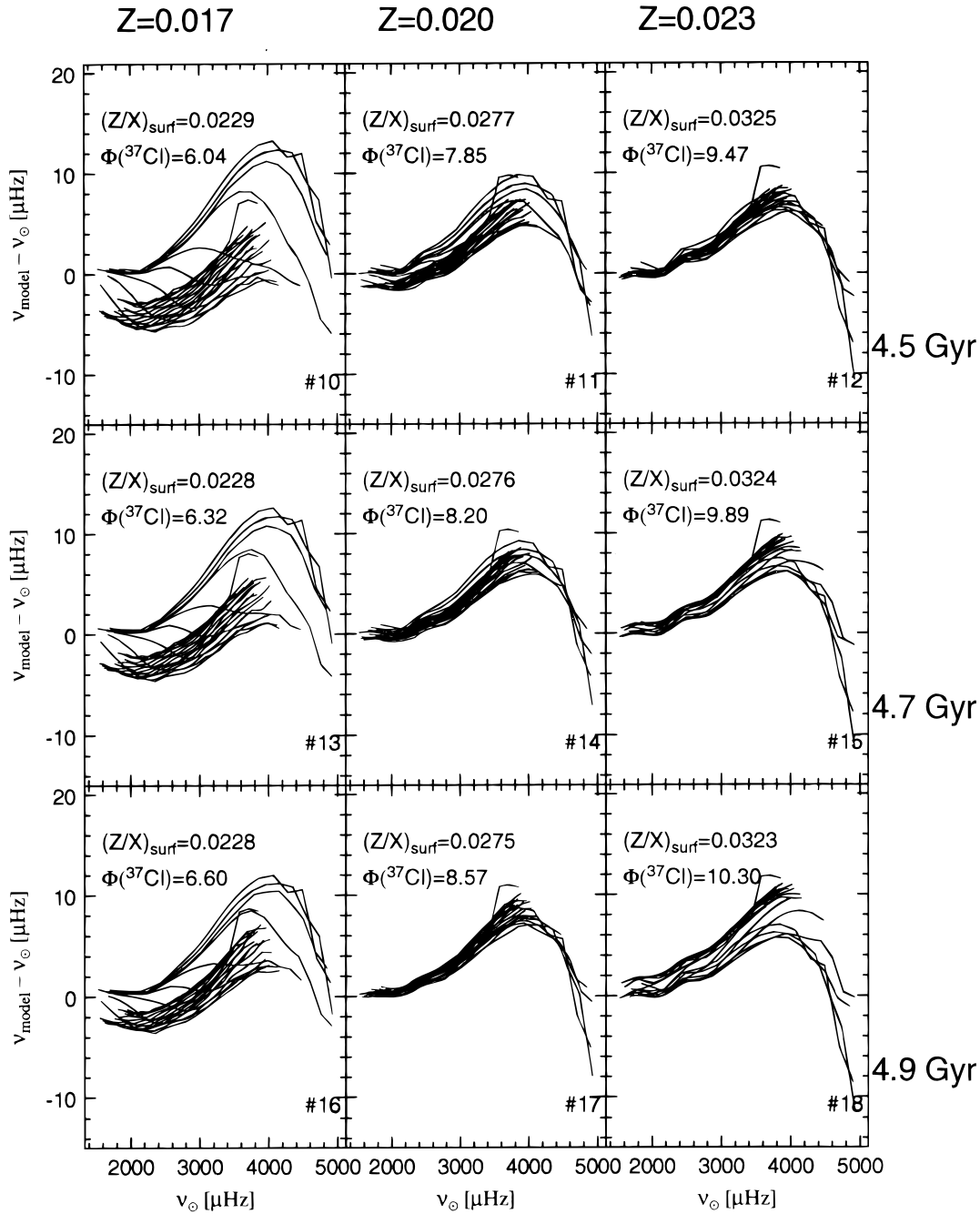


FIG. 3.—Grid of plots, each showing the p -mode frequency differences, model minus Sun, for models that include helium diffusion only. Each plot is annotated with the surface Z/X ratio and the ^{37}Cl neutrino flux, in SNU. The observational data are from GONG.

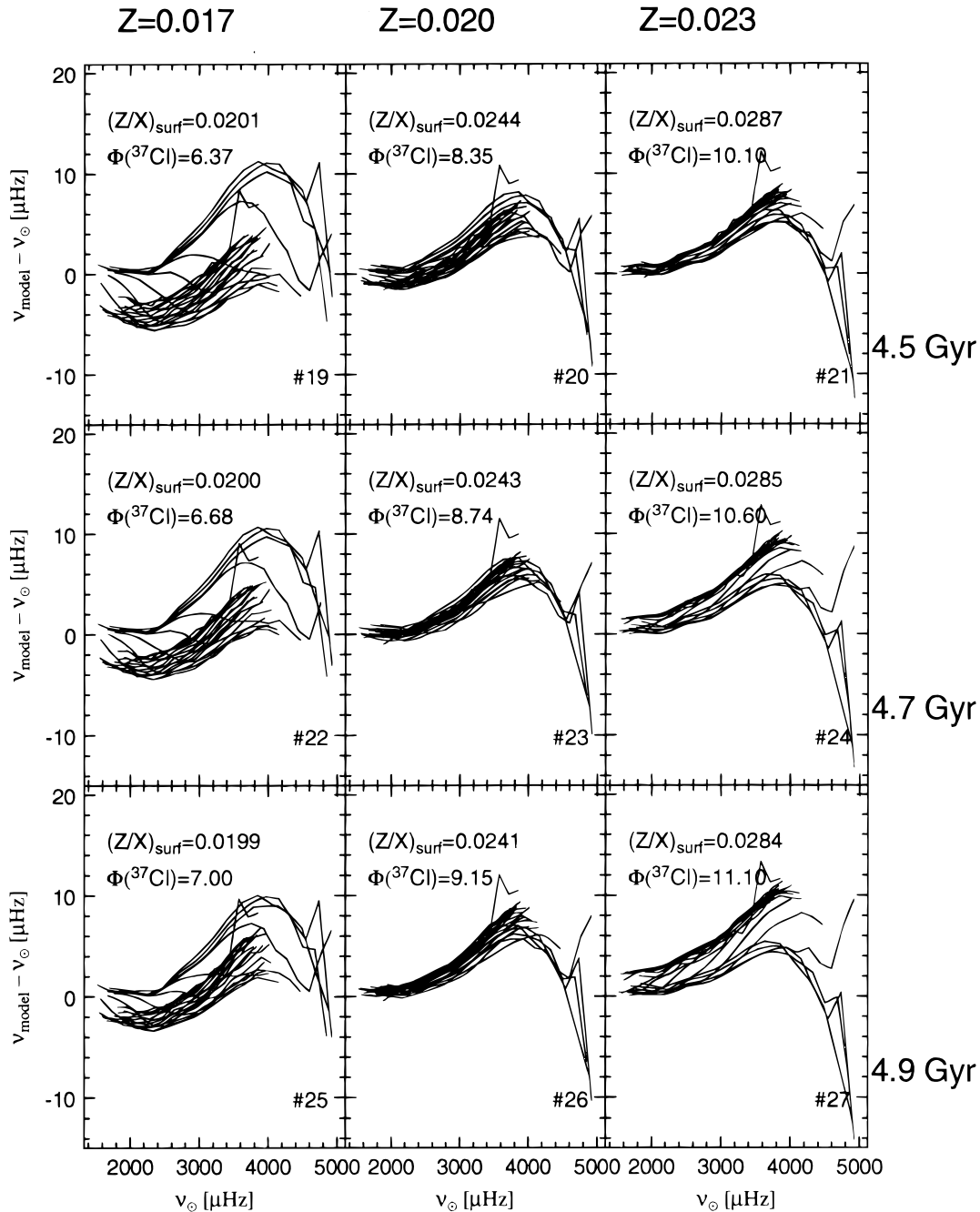


FIG. 4.—Grid of plots, each showing the p -mode frequency differences, model minus Sun, for models that include helium and heavy-element diffusion. Each plot is annotated with the surface Z/X ratio and the ^{37}Cl neutrino flux, in SNU. The observational data are from GONG.

the values of $(Z/X)_{\text{surf}}$ and ^{37}Cl neutrino flux for the corresponding model. These should be compared to the corresponding observed values: $(Z/X)_{\odot} = 0.0244 \pm 0.001$ (Gerevesse, Noels, & Sauval 1996) and $\Phi(^{37}\text{Cl}) = 2.32 \pm 0.26$ SNU (Davis 1993). If our solar models were in perfect seismic agreement with the Sun, the frequency differences for all of the p -modes would be zero, and all the data would lie on a straight horizontal line intercepting the ordinate axis at $0 \mu\text{Hz}$. The lines connect common l -valued p -modes, hence, group together p -modes that have approximately similar inner turning points. Only $l = 1-12, 15, 20, 25, 30, 35, 40, 50, 60, 80,$ and 100 are plotted. As explained in the introduction, known uncertainties in our treatment of the very outermost layers introduces a slope error, where

the discrepancy increases with increasing frequency. Ignoring this error, we judge the quality of the model by the thickness of the bundle of lines. The bundle thickness directly correlates to errors in the interior of the model, primarily errors near the base of the convection zone. If the lines are tightly bundled, then we conclude that the corresponding model is a good fit to the Sun in the region near and above the base of the convection zone.

The small spacing $\delta\nu$ is sensitive to the structure of the core. The sensitivity decreases with increasing l and the depth of the sensitivity also decreases with increasing l . As we show here, little information is obtained about the core from the small spacings of p -modes with l -values greater than 5.

In Figures 5, 6, 7, and 8 we show the small spacing differences (model minus Sun) for the $l = 0, 1, 5,$ and 10 small spacings, respectively. Each figure contains a 3×3 grid of plots, with each plot corresponding to a different age and diffusion combination. Each plot shows the small spacing differences for models with $Z = 0.017, 0.020,$ and $0.023,$ which are distinguishable by the different line styles used to connect the data points. The horizontal row of dots with error bars show the sum of the observed error in frequency of the $\nu(n, l)$ and the $\nu(n - 1, l + 2)$ p -modes used to calculate the observed small spacing. Clearly, agreement between

a model and the observation occurs when the small spacing differences fall inside the horizontal row of error bars. Note that the ordinate-axis scale for the $l = 5$ and 10 small spacing difference plots is one-half that of the $l = 0$ and 1 plots. For all the small spacing plots we use the GONG (Harvey et al. 1996) low- l p -mode results.

The $l = 5$ and 10 small spacing differences are nearly identical for all the models considered here. The errors are too large and the sensitivity too small to be a useful diagnostic of the core. For example, the $l = 10$ small spacings (Fig. 8) for the models are larger than the observed small

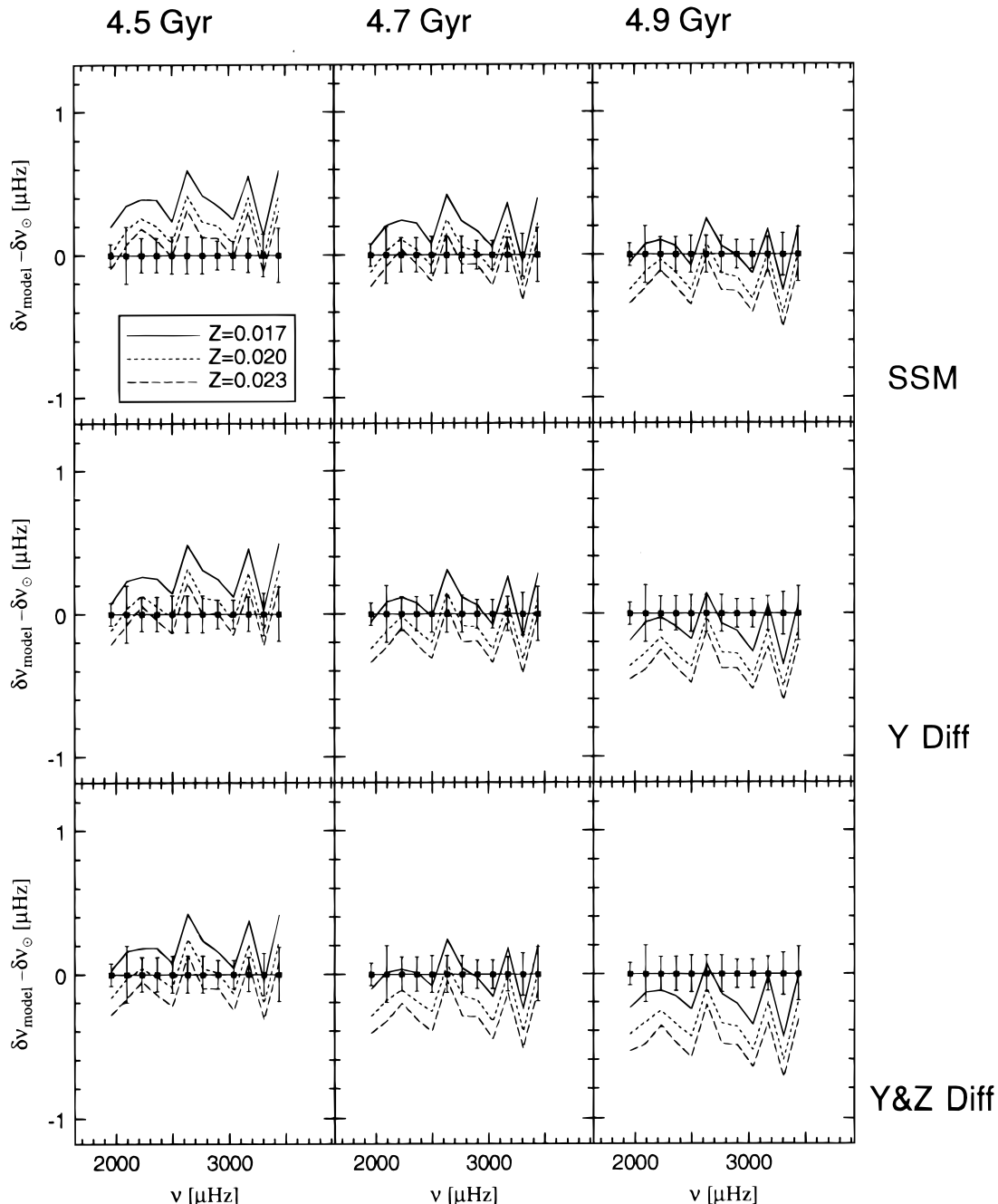


FIG. 5.—The $l = 0$ small spacing differences (see definition in text) are plotted against observed p -mode frequency for all the standard solar models (1–27 in Table 1). The horizontal row of data points with error bars, in each plot, defines the error associated with observed small spacing. “SSM,” “Y Diff,” “Y&Z Diff” define the rows of plots corresponding to models without diffusion, with helium diffusion only, and with helium and heavy-element diffusion, respectively. The observational data are from GONG.

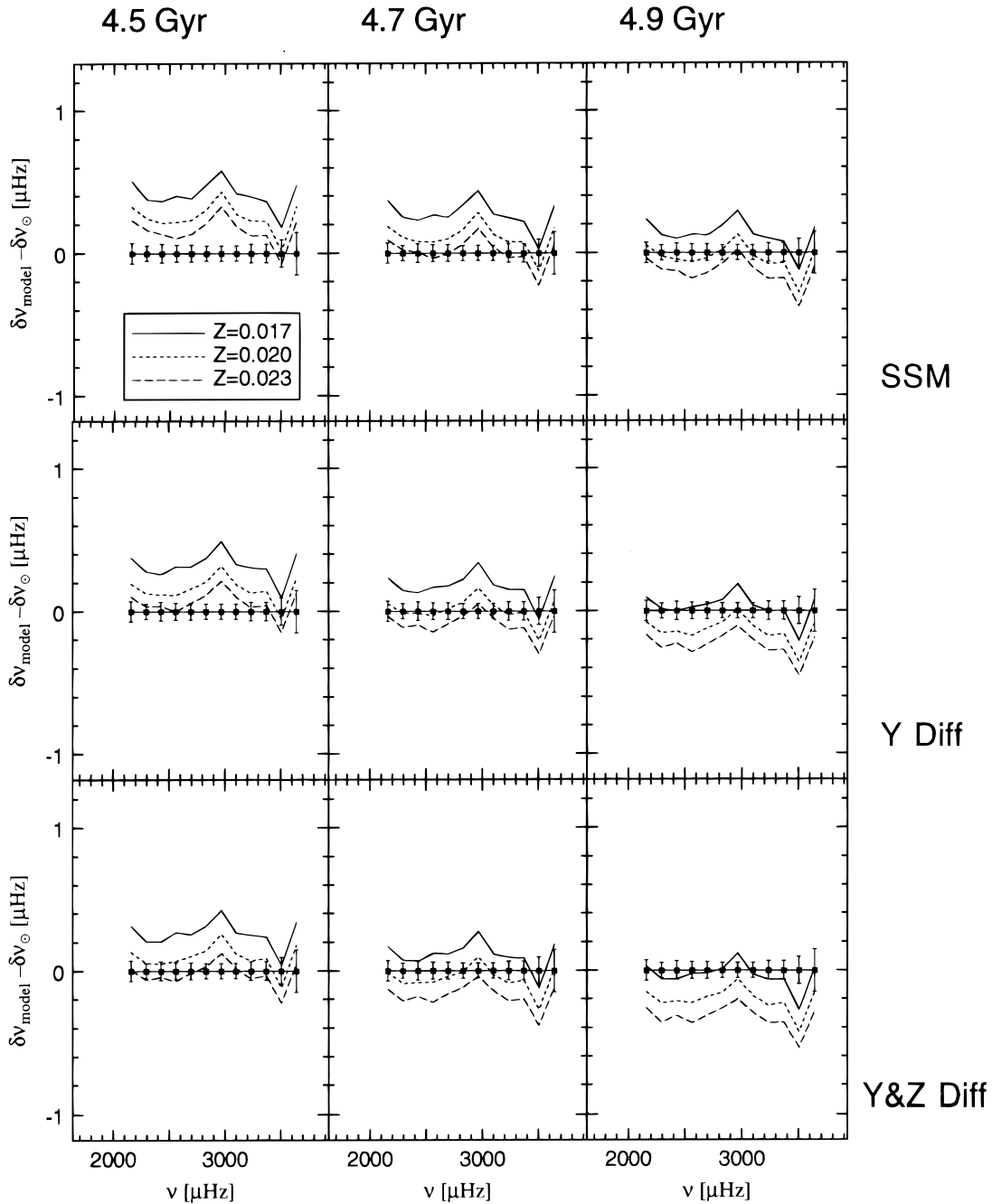


FIG. 6.—Similar to Fig. 5, except with $l = 1$ small spacing differences

spacings. As mentioned earlier, as l increases the sensitivity of the small spacing to the core decreases. At $l = 10$ the weak core sensitivity is over shadowed by the small spacing's growing sensitivity to the surface layers, which is responsible for most of the poor agreement.

As expected, the $l = 0$ and 1 small spacings are a more useful diagnostic of the core. Specifically, the small spacings are sensitive to the age of the model. This is because older models have greater mean molecular weights in the core (greater densities), which leads to lower sound speeds in the core ($c_s \propto \rho^{-1/2}$), hence, lower sound speed gradients, which, in turn, leads to lower p -mode frequency spacings (see eq. [2]). This is shown in Figure 9, a grid of plots of the sound speed c_s in the core as a function of radius fraction for all of the standard models (1–27).

3.4.2. Models with No Diffusion

Referring to Figure 2b, we see that models with the highest Z_{init} (0.023) have the most compact bundle of lines, hence, are in best agreement with the observed p -mode frequencies. But we also see that the models with $(Z/X)_{\text{surf}}$, closest to the observed value, $(Z/X)_{\odot} = 0.0244$, having $Z_{\text{init}} < 0.020$, have the poorest agreement with the observed p -mode frequencies. A solar model that does not include any diffusion, regardless of age, cannot be made to match both the observed p -mode frequencies and the observed $(Z/X)_{\odot}$ —agreement with one observable compromises the agreement with the other.

Referring to Table 1, we see that the radius fraction location of the base of the convection zone R_{env} is closest to the

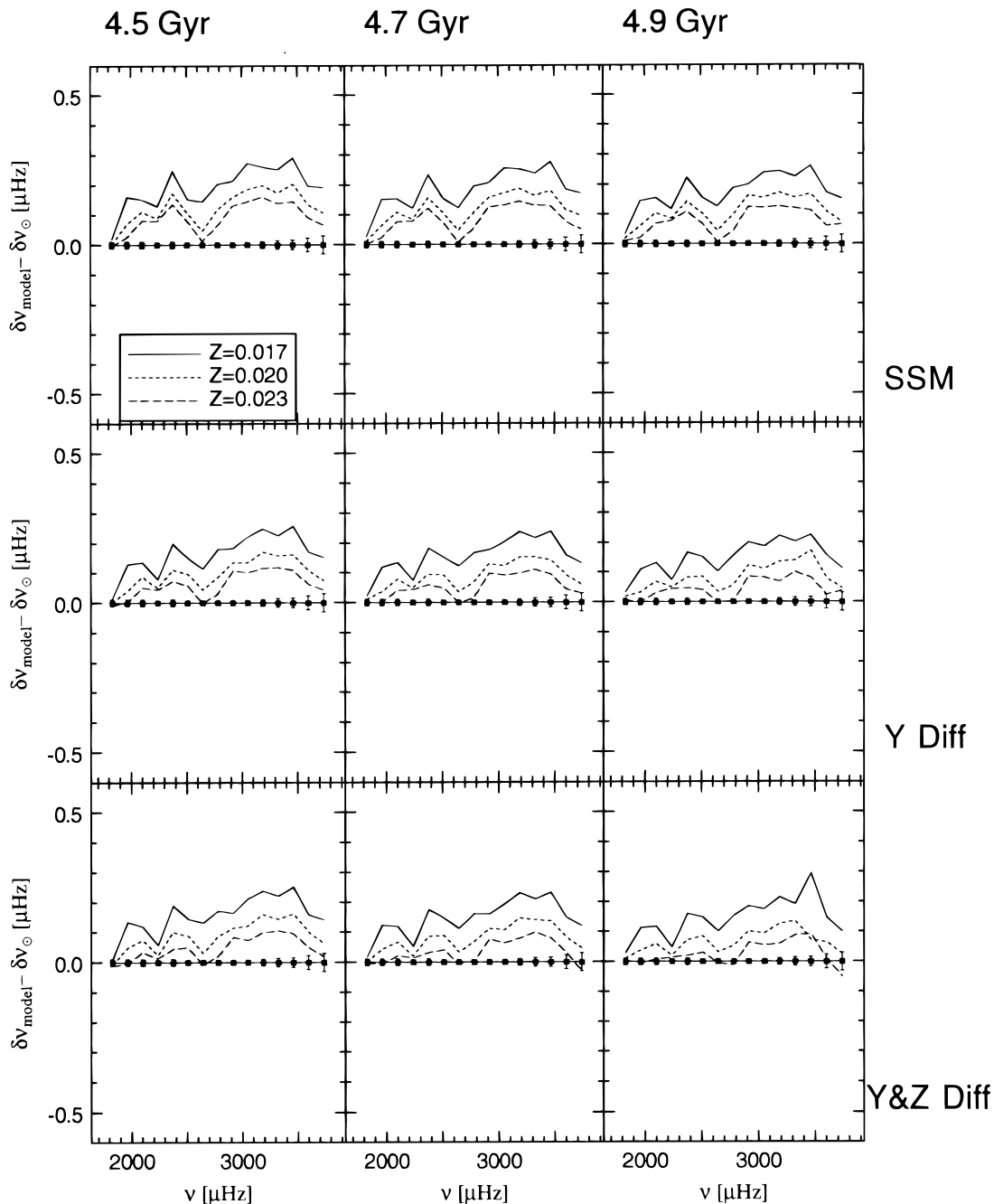


FIG. 7.—Similar to Fig. 5, except with $l = 5$ small spacing differences

depth determined by Christensen-Dalsgaard et al. (1991) via seismic inversion, 0.713 ± 0.003 , for the high- Z models. This is entirely consistent with the results of Figure 2b, in that the $l = 30\text{--}50$ p -modes have inner turning points near the base of the convection zone. An incorrectly located convection zone base will maximally perturb the frequencies of these modes, and this will show up as an increase in the bundle thickness, with $l < 50$ modes affected by the location of the convection zone base and $l > 50$ modes (turning points above the convection zone base) unaffected (see, for example, discussion in Guenther 1994).

The small spacing difference plots for these models (top row of plots in Figs. 5, 6, 7, and 8) show that only the 4.7 Gyr models fit the observations within the error bars. This

age is significantly greater than the meteoritic age of the sun (4.53 ± 0.04 Gyr).

With current physics, but excluding diffusion, a standard solar model cannot be constructed to match simultaneously the observed $(Z/X)_{\odot}$, the meteoritic solar age, and the p -mode frequencies.

3.4.3. Models with Helium Diffusion

Including helium diffusion in the standard solar model calculation does decrease the degree of the incompatibility but does not eliminate it. In Figure 3 we show frequency difference plots for all the models that include helium diffusion (only). The best models in this group, i.e., the models in Figure 3 that have the tightest line bundles, are models 12,

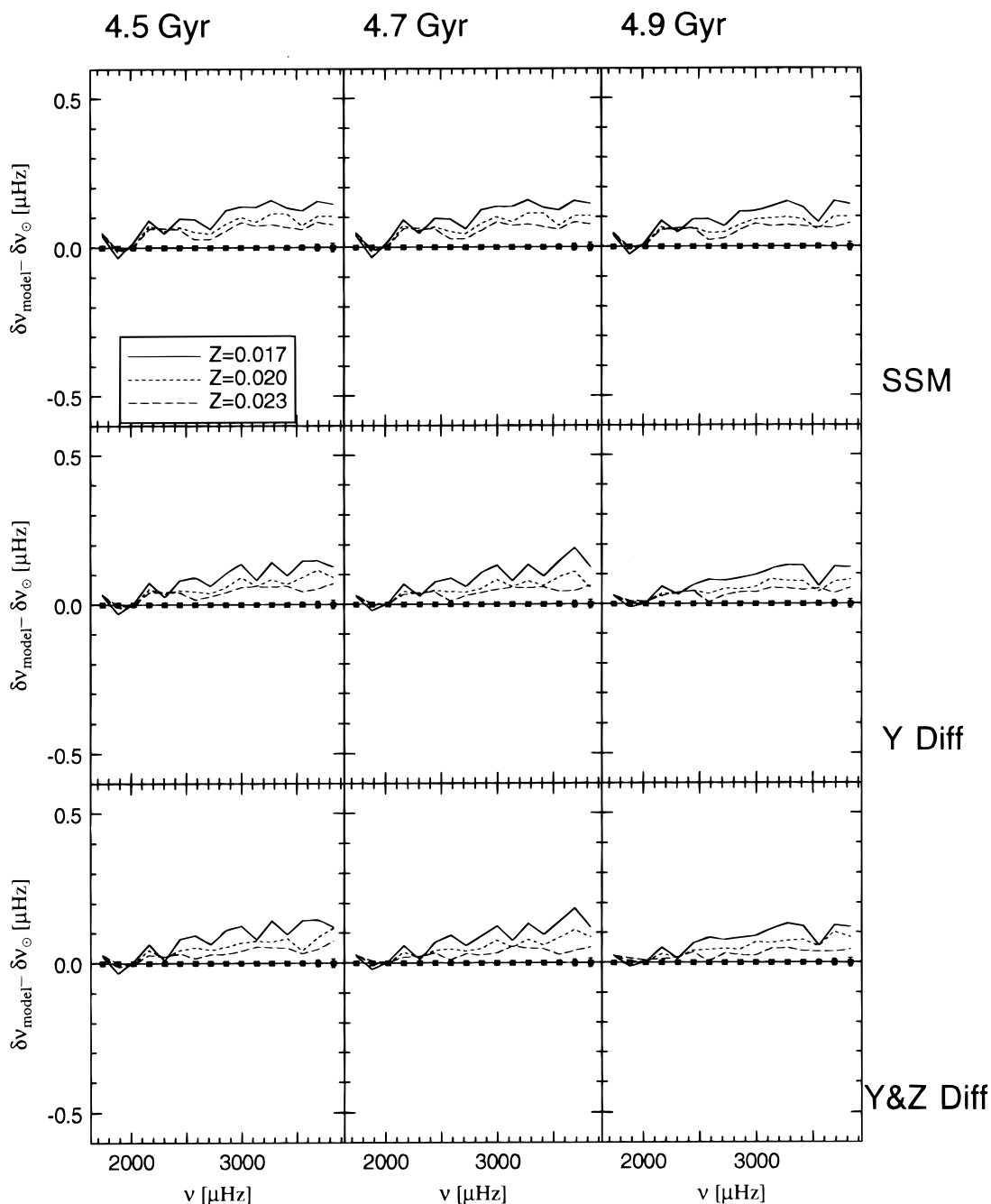


FIG. 8.—Similar to Fig. 5, except with $l = 10$ small spacing differences

14, and 17. They also have convective envelope depths (0.711, 0.713, 0.711, respectively) that most closely match the seismic depth, 0.713 (Christensen-Dalsgaard, Proffitt, & Thompson 1993). All of these models, though, have $(X/Z)_{\text{surf}}$ greater than the observed value.

Although our grid is coarse, it still appears that the optimum choice of models with regard to $(Z/X)_{\text{surf}}$ does not intersect the optimum choice of models with regard to p -mode frequencies. The intersection occurs for models that are about 4.7 Gyr old.

Including helium diffusion in the model is similar to increasing the aging rate of the model. As helium slowly diffuses inward, the mean molecular weight in the core increases at a slightly higher rate, as the model evolves, than if diffusion were not present. Effectively the core ages, i.e.,

helium is built up in the core, faster when helium diffusion is included. Including helium diffusion, therefore, decreases the sound speed in the core (see Fig. 9) which decreases the frequencies and their separations. The effects of age and diffusion on the small spacings can be seen in Figures 5 ($l = 0$) and 6 ($l = 1$). As the age is increased, or as helium diffusion is included in the model, the model minus observed small spacings decreases. Agreement with the small spacings occurs at a lower age, compared to solar models that do not include helium diffusion.

3.4.4. Models with Helium and Heavy-Element Diffusion

In Figure 4 we show the frequency differences for models with helium and heavy-element diffusion. Because metals settle out of the surface convection, $(Z/X)_{\text{surf}}$ is reduced,

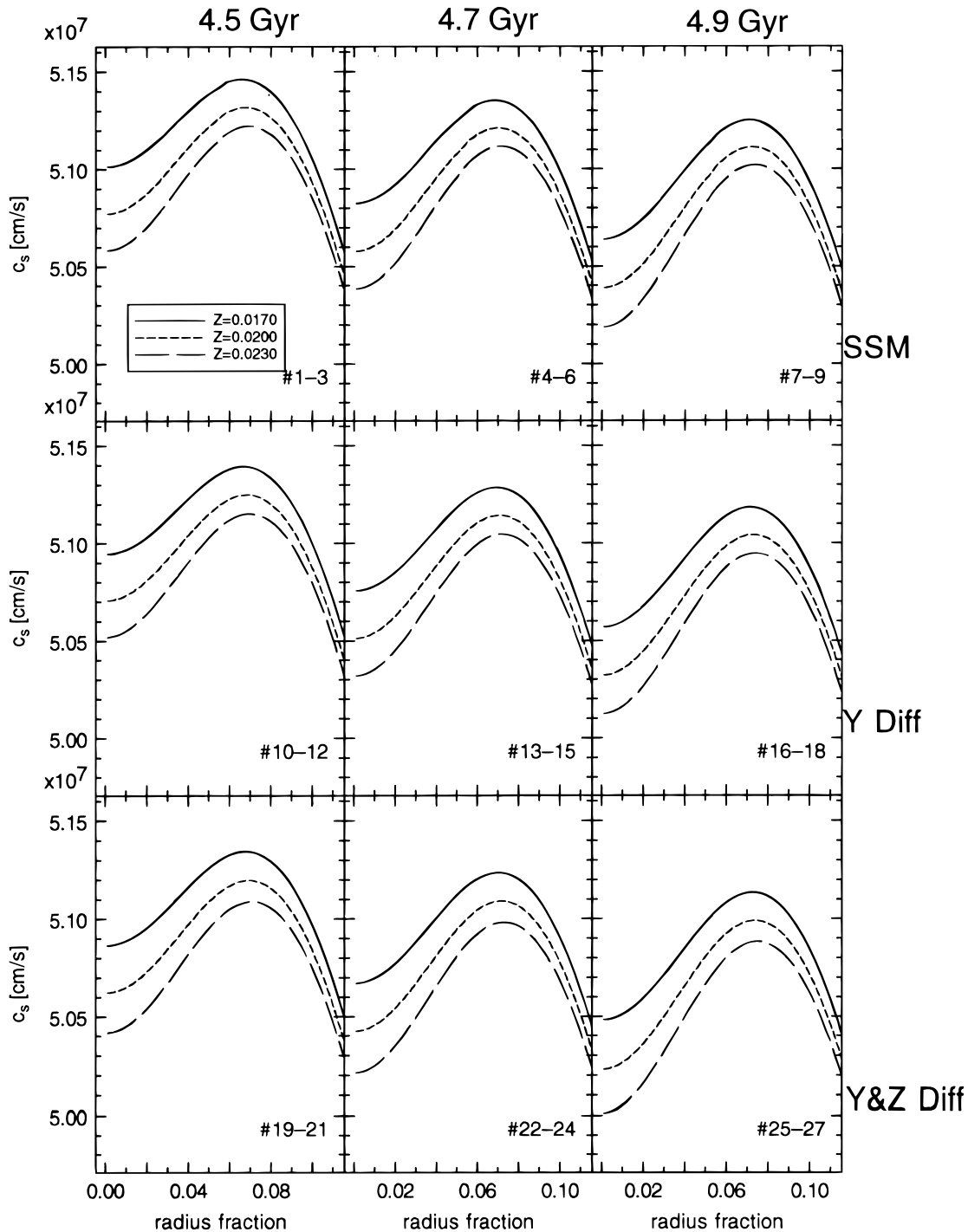


FIG. 9.—Run of sound speed in the core for all the standard solar models (1–27) in Table 1) against radius fraction. “SSM,” “Y Diff,” and “Y&Z Diff” define the rows of plots corresponding to models without diffusion, with helium diffusion only, and with helium and heavy-element diffusion, respectively.

while Z/X in the interior, where it affects the p -mode frequencies, is only slightly increased. Consequently, the $Z_{\text{init}} = 0.020$ models have $(Z/X)_{\text{surf}}$ nearly equal to $(Z/X)_{\odot}$ and at the same time have p -mode frequencies that are in good agreement with the observed p -mode frequencies. Based on these two criteria only, we would select the best models to be in the age range 4.5–4.9 Gyr with Z_{init} in the range 0.019–0.021. The uncertainty ranges are large, primarily a consequence of our uncertainty in the surface boundary conditions of the solar models (owing to uncertainties in our modeling of convection, atmospheres, and

opacities). Regardless, the data show that the inclusion of heavy element diffusion resolves the problem of incompatibility between the preferred “ $(Z/X)_{\text{surf}}$ ” models and the preferred “ p -mode frequency difference” models that exists for the models that have no diffusion or include only helium diffusion.

When heavy element diffusion is included in the model, the small spacings decrease. The core helium abundance of the solar model that includes Z diffusion must increase relative to a model that does not because the slightly larger values of Z in the core increase the opacity there. This

demands a compensating increase in central luminosity to maintain the observed photon luminosity. We bring about this change by increasing the central abundance of helium. As a consequence, including Z diffusion, decreases the central sound speed (see Fig. 9), which decreases the small spacings.

We have already concluded that agreement with the observed $(Z/X)_{\odot}$ can only be obtained for models that include helium and heavy-element diffusion, therefore, we will focus our attention on these models, represented in the last row of the plots in Figures 5, 6, 7, and 8. We see that none of the 4.9 Gyr models have small spacings in agreement with observations. At 4.7 Gyr, the small spacings agrees best for the model with $Z_{\text{init}} = 0.017$ (model 22), but $(Z/X)_{\text{surf}} = 0.020$, which is too low. At 4.5 Gyr, the small spacings agrees best for model 20 where $Z_{\text{init}} = 0.020$ and $(Z/X)_{\text{surf}} = 0.0244$, which is precisely the observed ratio. Estimating the error in the seismic age of the Sun to be about ± 0.1 Gyr, we conclude that the resulting seismic age of the Sun is 4.5 ± 0.1 Gyr, in excellent agreement with the solar age derived from meteoritic data (4.53 ± 0.04 Gyr). Thus the small spacings derived from the GONG data confirm with remarkable precision the validity of solar models based on the standard theory of stellar evolution, provided the effects of helium and heavy element diffusion are included.

4. NONSTANDARD SOLAR MODELS

4.1. Low- Z Core Models

Some unconventional scenarios of the formation of the Sun in which heavy elements locked up in grains are segregated from the hydrogen and helium gas in the presolar

nebula have been advanced, as well as scenarios in which the Sun is formed by accretion to an initial core of different chemical composition (e.g., Prentice 1973; Hoyle 1975). These scenarios have remained a frequently mentioned option for the solution of the solar neutrino problem (Rood 1978) because it was realized that models in which hydrogen burning takes place at lower temperatures than in standard models have lower neutrino fluxes. Despite the fact that low- Z models are contrary to the notion that elements heavier than hydrogen will sink toward the center of the gravitational potential, and are implausible on other astrophysical grounds, they have remained popular until this day because they could not be ruled out by direct observations of the Sun (Christensen-Dalsgaard 1992).

We have calculated a variety of low- Z core models (see models 48–54 in Table 2), each with near-zero metallicity extending outward to a specified mass M , ranging from 0.02 to $0.20 M_{\odot}$. All the models were evolved to 4.7 Gyr and include the effects of helium and heavy-element diffusion, i.e., they should be compared to the standard model 23. The effect of the low- Z core assumption on the p -mode frequencies is not easily discernible in the frequency difference plots (hence, is not shown here) but is noticeable in the small spacing difference plots. Figure 10 shows the small spacing differences for selected l -values for all of the low- Z core models calculated. As noted in § 2.2, the $l = 5$ and 10 small spacings are subject to uncertainties in the surface layers of the model and are not effective probes of the core. However, the $l = 0$ and $l = 1$ small spacings effectively rule out low- Z cores extending beyond $0.06 M_{\odot}$.

In Figure 11 we plot the extent of the low- Z core versus the predicted flux for ^{37}Cl detectors. As the low- Z core

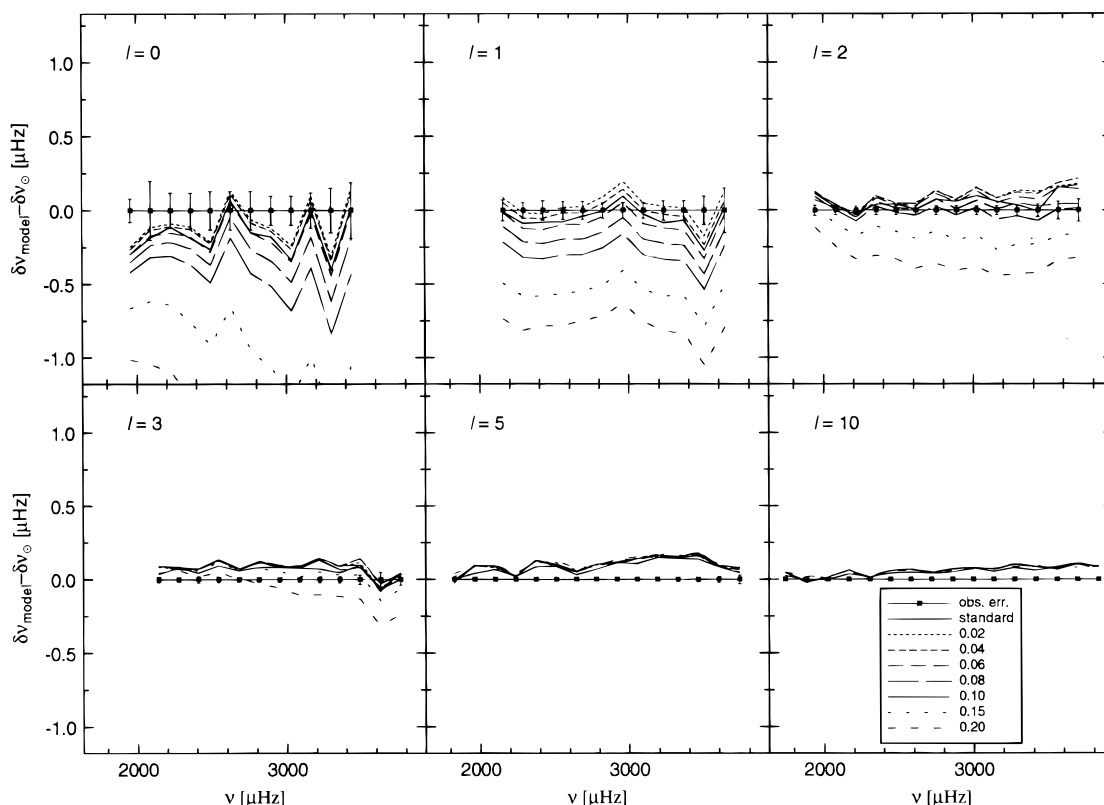


FIG. 10.—Small spacings for the nonstandard solar models with low- Z cores (48–54 in Table 2). The extent of the low- Z core, in mass fraction, for each model is indicated in the legend. The horizontal row of data points with error bars, in each plot, defines the error associated with observed small spacing. The observational data are from GONG.

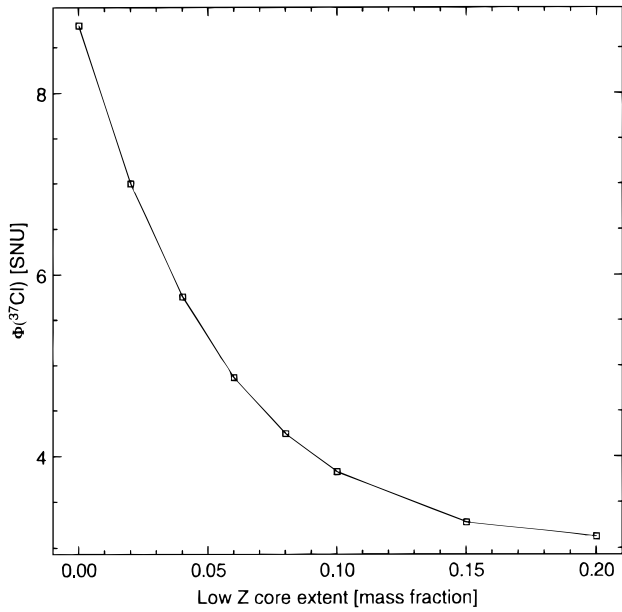


FIG. 11.—Predicted neutrino fluxes for ^{37}Cl detectors vs. the extent of the low-Z core (in the nonstandard solar models).

region is extended the neutrino flux is reduced. Similar neutrino flux reductions occur for ^{71}Ga (see Table 2 and 4). We see that the small spacing observations, which rule out low-Z cores extending beyond $0.06 M_{\odot}$, also rule out any

chance that a low-Z core model could reduce the neutrino flux below ~ 4.87 ^{37}Cl SNU and ~ 119 ^{71}Ga SNU.

4.2. Mixed-Core Models

Another class of nonstandard solar models long-favored to explain the solar neutrino observations is one in which the central region of the Sun, where the energy generation takes place, is mixed. The main idea is that mixing results in a lower central helium content, a lower mean molecular weight and temperature at the center, and therefore a reduced predicted neutrino flux (Bahcall et al. 1968; Ezer & Cameron 1968). These types of models have been reconsidered in various forms over the years.

We have calculated a grid of mixed core models with the extent of the mixed region ranging from 0.01 to $0.5 M_{\odot}$ (see models 28–38 in Table 2 and 4). All the models were evolved to 4.7 Gyr and include the effects of helium and heavy-element diffusion (hence, should be compared to standard model 23). The bundle thickness of the p -mode frequency differences, shown in Figure 12, can be used to rule out the most extreme of these cases, that is, the models in which the mixed core extends beyond $0.2 M_{\odot}$. Referring to Table 4, we see the bundle thickness of the p -mode frequency differences directly correlates to how near the base of the convection zone in the model is to the depth determined from seismic inversions ($0.713 R/R_{\odot}$).

In Figure 13, we plot the predicted neutrino flux, $\Phi(^{37}\text{Cl})$, opposite the extent of the mixed core. Because the p -modes enable us to rule out models with mixed cores extending

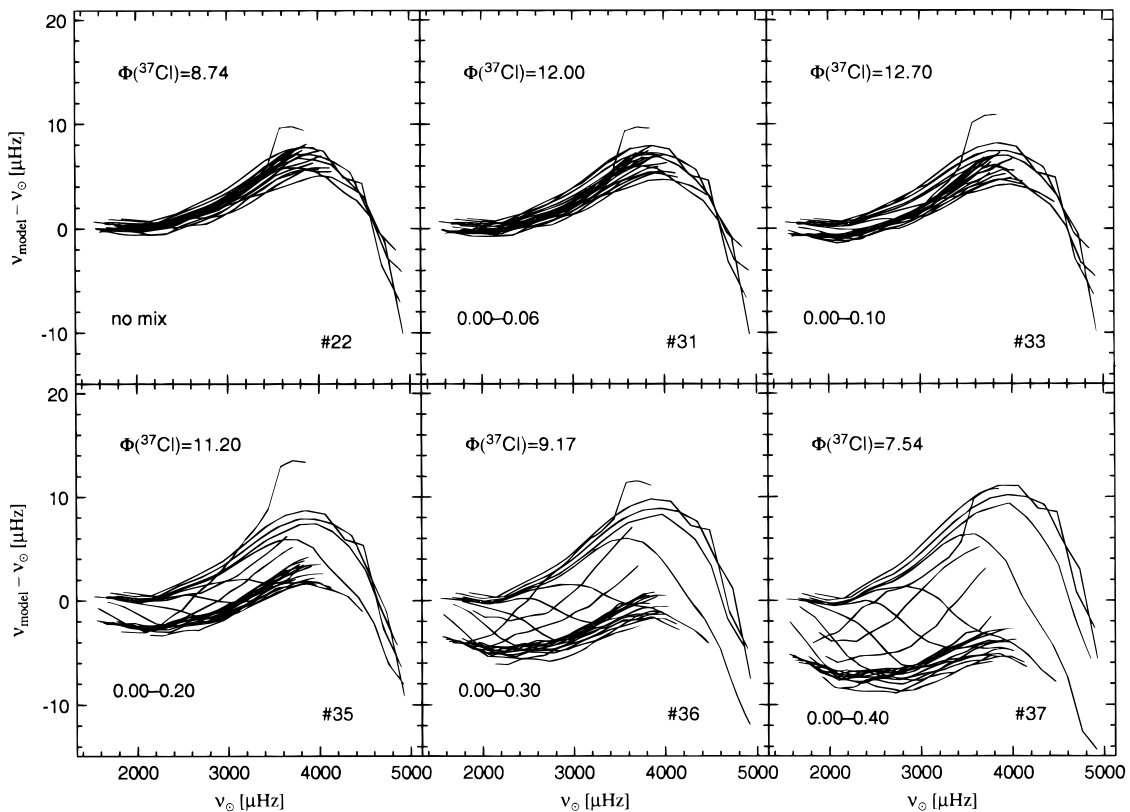


FIG. 12.—Grid of plots, each showing the p -mode frequency differences, model minus sun, for models with mixing forced to occur in the core and for the standard solar model 23. Each plot is annotated with the ^{37}Cl neutrino flux, in SNU, and the extent of the mixed region, in mass fraction. All models include the effects of helium and heavy-element diffusion, with $Z_{\text{init}} = 0.020$ and a final age of 4.7 Gyr. The observational data are from GONG.

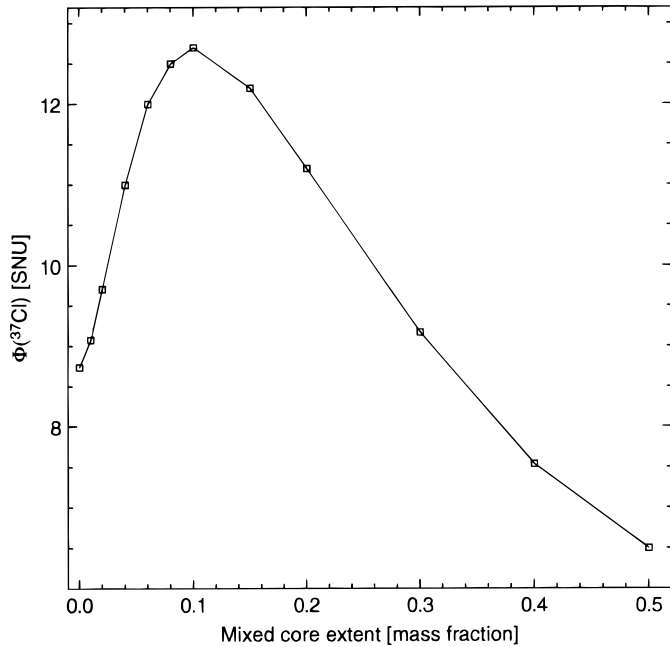


FIG. 13.—Predicted neutrino fluxes for ^{37}Cl detectors vs. the extent of the mixed core.

beyond $0.2 M_{\odot}$ we have effectively ruled out any possibility that the mixed-core scenario can be used to reduce the neutrino flux the $\Phi(^{37}\text{Cl})$ does not drop below ~ 9 SNU for mixed core models extending short of $0.2 M_{\odot}$. Only for

models with mixed cores extending beyond $0.3 M_{\odot}$ is there any reduction in the neutrino flux, and even with mixed regions extending out to $0.5 M_{\odot}$ the reduction is only to $6.5 ^{37}\text{Cl}$ SNU.

Mixed core models have been studied in other contexts outside the solar neutrino problem. For example, because a mixed core extends the main-sequence lifetime of the star, as new hydrogen fuel is mixed into the central burning regions of the star, mixed core models have been discussed in the context of globular cluster ages and even blue stragglers (Wheeler 1979). It is therefore interesting to know if even a small mixed core is tolerated by the p -mode frequencies in the solar model. We use the small spacings to place a constraint on the extent of a mixed core in the Sun.

In Figure 14 we show the small spacings for all of the mixed core models extending out to $0.1 M_{\odot}$. The $l = 1$ small spacing is particularly sensitive to mixing in the core. As seen in Figure 14, the $l = 1$ small spacing results enable us to rule out the possibility of a mixed core extending beyond $0.02 M_{\odot}$.

4.3. Mixed Shell Models

Based on the results described in the § 4.2 there is no reason to believe that mixing in an envelope will have a stronger effect in reducing the neutrino flux than mixing all the way to the center. Regardless, it is interesting in the context of stellar seismology to know how extensive a mixed region is tolerated in a star before its effects are noticeable in the p -mode frequencies.

Mixing could be a possible outcome of the so-called “spoon” due to the ^3He instability, and it could occur

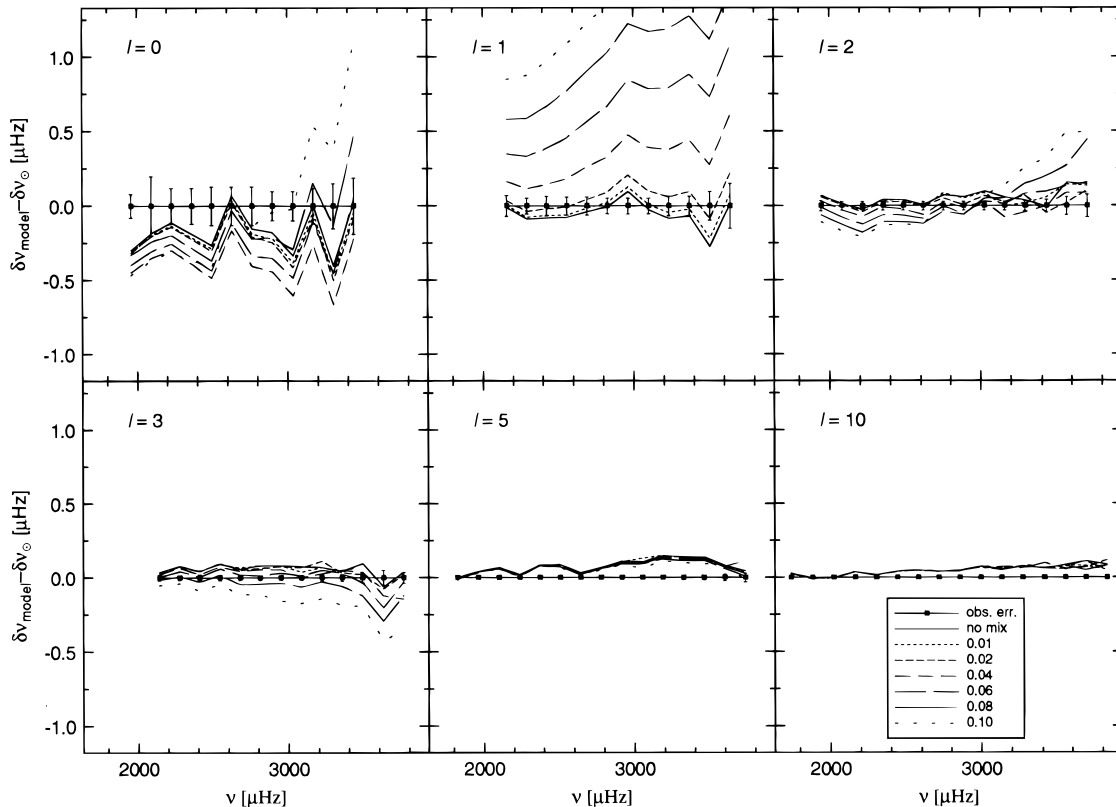


FIG. 14.—Small spacings for the nonstandard solar models with mixed cores (28–33 in Table 2). The extent of the mixed core, in mass fraction, for each model is indicated in the legend. The horizontal row of data points with error bars, in each plot, defines the error associated with observed small spacing. The observational data are from GONG.

either continuously or sporadically in the solar interior (Dilke & Gough 1972). We discuss this case because envelope mixing has been proposed at various times as a method to alter the ratio of the ${}^7\text{Be}/{}^8\text{B}$ flux, needed to reconcile the model predictions with observations. Recently, Cumming & Haxton (1996) have proposed a circulation scheme in the solar interior which proceeds at just the right rate to move material from the ${}^3\text{He}$ peak down into deeper layers on a timescale of the same order of magnitude as for ${}^3\text{He}$ to reach burning equilibrium. This scheme has the advantage of decreasing the ${}^7\text{Be}/{}^8\text{B}$ neutrino flux ratio. Because this scheme has not been included in a consistently tuned solar model, it is unclear how much the neutrino fluxes themselves would be decreased by this mixing. The Cumming-Haxton scheme differs from the mixing scheme we use here (in which we assume that the mixing takes place instantaneously), and, as a result, our models do not modify the ${}^7\text{Be}/{}^8\text{B}$ appreciably. But because the mean molecular weight and the internal structure are primarily affected by the mixing of ${}^4\text{He}$ (which must take place at the same time as the proposed ${}^3\text{He}$ mixing), our shell-mixed solar models should be similar to the Cumming-Haxton models from the point of view of seismology.

From Table 2 and 4, we see that none of the mixed envelope models calculated (models 42–50) are effective in significantly reducing the total neutrino flux. In addition, the ratio of the ${}^7\text{Be}/{}^8\text{B}$ flux (see Table 4) is not significantly altered.

In Figures 15, 16, and 17 we plot the small spacings for all the mixed envelope models. The base of the mixed envelope

is located at 0.05 , 0.10 , and $0.20 M_{\odot}$, for Figures 15, 16 and 17, respectively. Notice that as the lower edge of the mixed envelope is pushed outward, first the $l = 3$, then the $l = 2$, the $l = 1$, and finally the $l = 0$ small spacings become less and less sensitive to the mixing. In Figure 15, corresponding to mixed envelope models with mixing bases at $0.05 M_{\odot}$, the small spacings, especially $l = 0$ and 1 , strongly rule out an outer mixed edge beyond $0.1 M_{\odot}$. In Figure 16, corresponding to a inner boundary for the mixed region at $0.1 M_{\odot}$, the $l = 2$ and 3 small spacings are less sensitive to the structural changes caused by the mixing and only the $l = 0$ small spacing is effective at constraining the extent of the mixed region. Mixed envelopes extending beyond $0.15 M_{\odot}$ are ruled out by the small spacings. This strongly argues against the extensive slow mixing needed to depress the ${}^7\text{Be}/{}^8\text{B}$ flux ratio, as proposed by Cumming & Haxton (1996). More detailed simulations, though, would be needed to completely rule it out. In Figure 17, the models have mixed region bases at $0.2 M_{\odot}$. The small spacings are not as sensitive to mixing in this region and can only constrain the mixing extent to $\leq 0.4 M_{\odot}$.

The small spacings tell us that if mixed envelopes exist they must be relatively thin. When the mixed region extends less and less into regions altered in composition by nuclear reactions, its effect on the structure is less, and so is the ability of the small spacings to detect the existence of the shell mixing. Thus, if slow mixing in a shell takes place in the Sun, it is either confined to a narrow region or exists in a region which is already nearly chemically homogeneous. Direct measurements of Doppler shifts of the oscillation

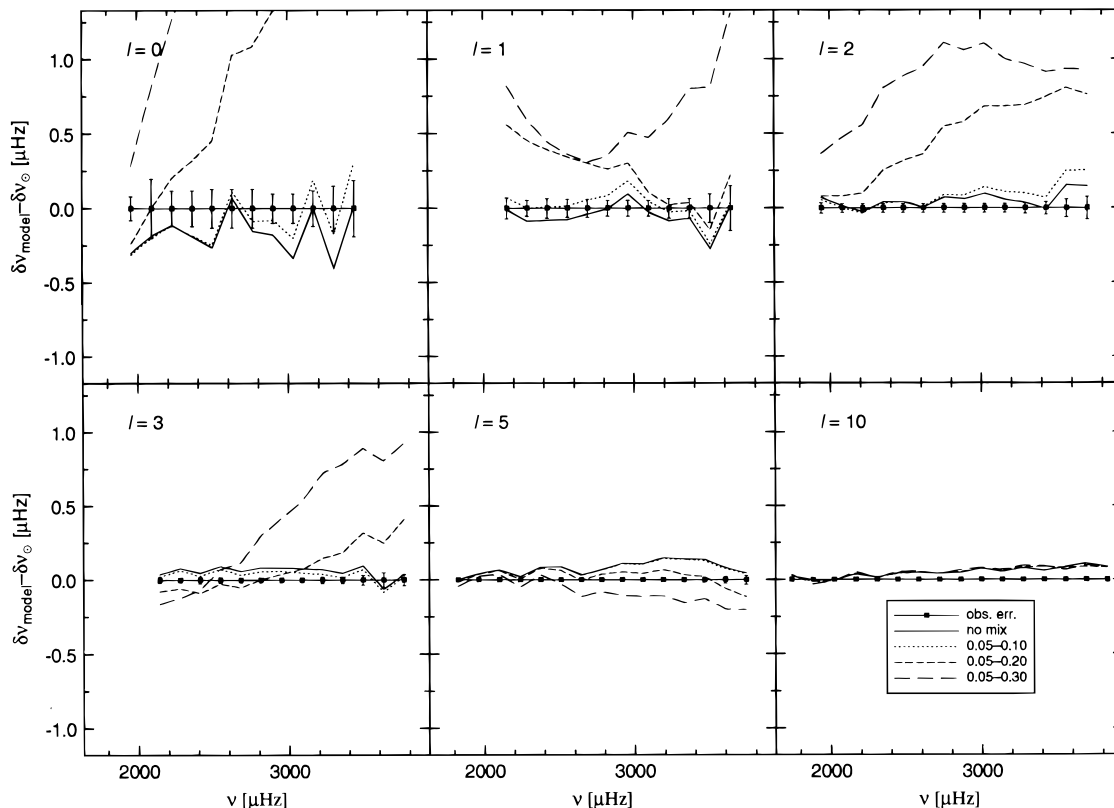


FIG. 15.—Small spacings for the nonstandard solar models with a mixed region (mixed shell) in the envelope (34–37 in Table 2). The base of the mixed region in these models is at $0.05 M_{\odot}$. The extent of the mixed envelope, in mass fraction, for each model is indicated in the legend. The horizontal row of data points with error bars, in each plot, defines the error associated with observed small spacing. The observational data are from GONG.

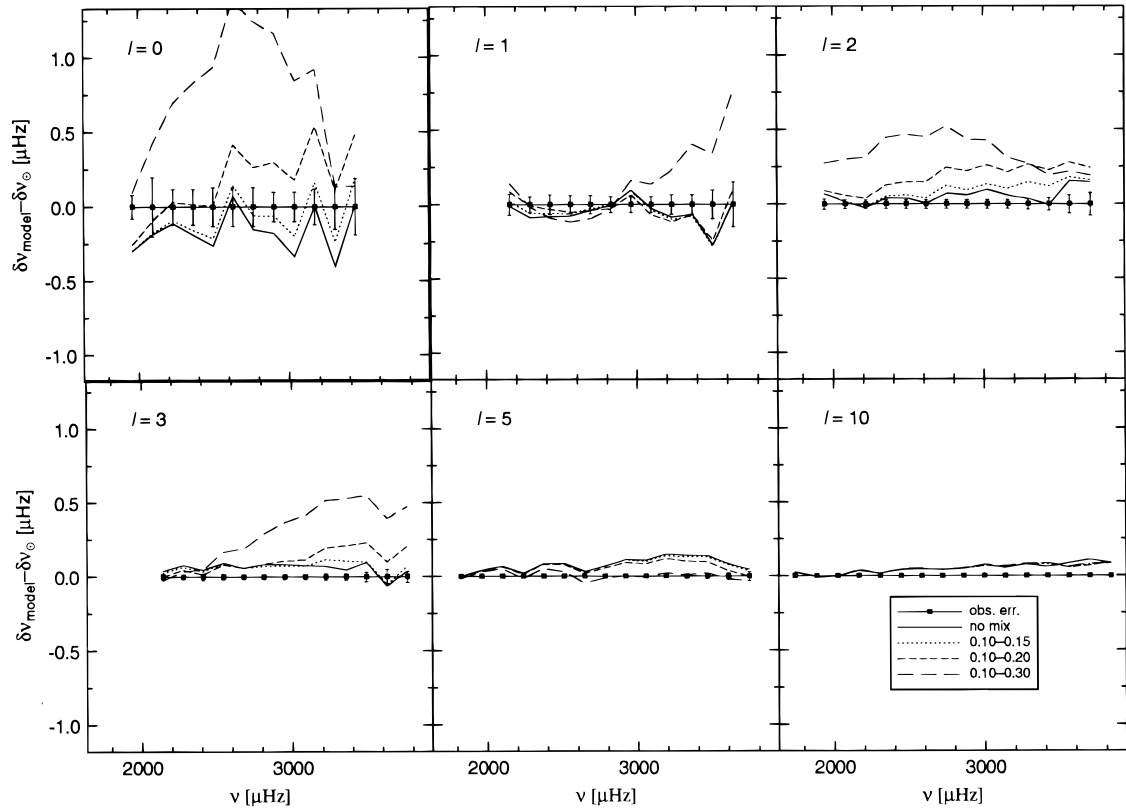


FIG. 16.—Similar to Fig. 15, except that the inner boundary of the mixed region starts at $0.10 M_{\odot}$

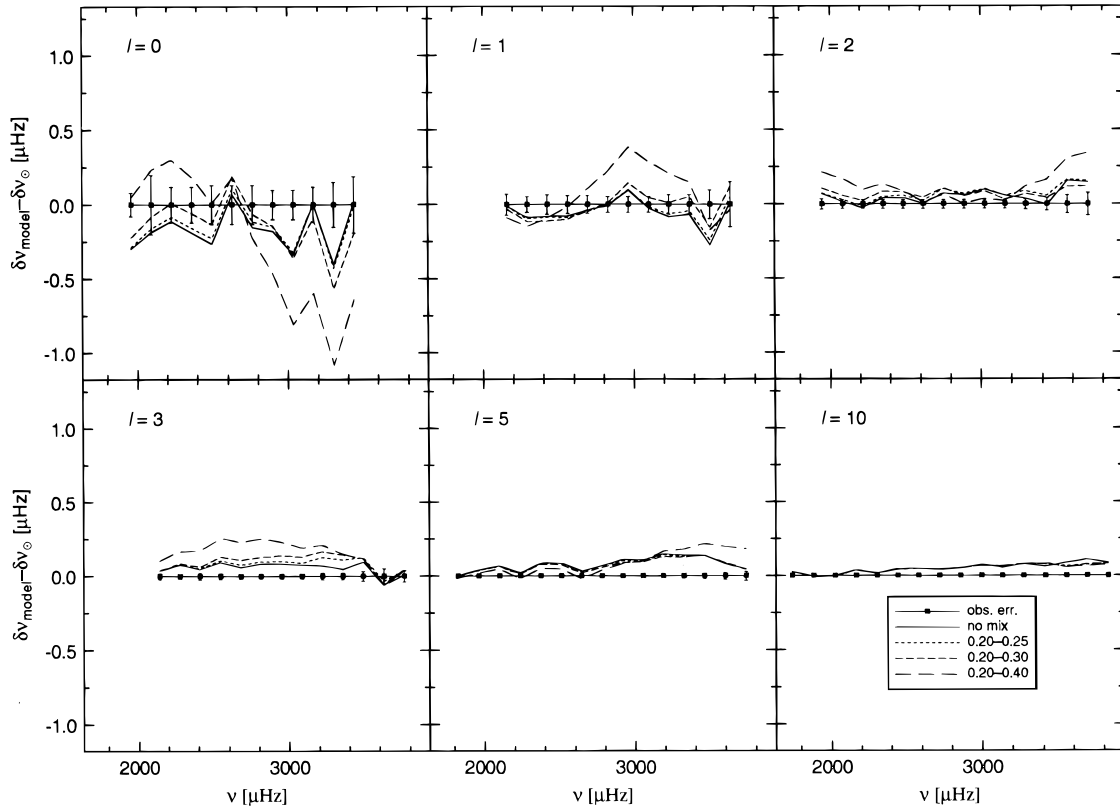


FIG. 17.—Similar to Fig. 15, except that the inner boundary of the mixed region starts at $0.20 M_{\odot}$

mode frequencies could in principle discern such motions, unfortunately the velocities are too small to be detectable with current technology. Even though mixing in chemically homogenous regions has little if any impact on the evolution of a star it could have an effect on the distribution and evolution of angular momentum in the star, the mixing of trace elements to the surface, and the existence, location, and evolution of magnetic fields (see, e.g., Chaboyer et al. 1995b for a description of the combined effects of rotational mixing and diffusion in an evolving solar model).

5. SUMMARY AND CONCLUSIONS

In the first part of this paper, we have presented three sets of evolved solar models under the standard assumptions, all finely tuned to the observed solar radius and luminosity. In each set, we have included in the models (1) no element diffusion, (2) helium diffusion, and (3) a treatment of the diffusion of both helium and the heavy elements, respectively. In addition, in each of the above cases, models were constructed for three initial heavy-element contents for the Sun (each yielding a surface value of $(Z/X)_{\text{surf}}$), and three ages near the age derived from the meteoritic age. The p -mode oscillation spectrum was then calculated for each solar model in the grid. An analysis was then carried out of the derived $(Z/X)_{\text{surf}}$ values and ages for the best fitting models. The quality of the helioseismic fit was based on two criteria: the differences between the observed and calculated frequencies and the differences between observed and calculated small spacings. Finally, for each model, and as a preparation for the second part of this paper, the predicted neutrino fluxes for each model was evaluated.

Our main conclusions are the following:

1. A standard solar model that does *not include element diffusion*, regardless of its assumed age, cannot be made consistent with both the observed p -mode frequencies and the observed $(Z/X)_{\odot}$.
2. *Including helium diffusion* in the standard solar model lessens the incompatibility with $(X/Z)_{\odot}$, but we note that the best fitting models have ages of 4.7–4.9 Gyr, well above the accepted meteoritic age of the solar system.
3. The *inclusion of both helium and heavy-element diffusion* removes the discrepancy between the best models implied by the p -mode frequency differences and the best models implied by $(Z/X)_{\odot}$. This is achieved for an age of the Sun (seismic age) of 4.5 ± 0.1 Gyr. The seismic age is in excellent agreement with the meteoritic age of the Sun, which is estimated at 4.53 ± 0.04 Gyr. This remarkable agreement would not have been possible without the spectacular advances in stellar physics of the last few years (opacities, equations of state, diffusion coefficients) and the high-quality data from GONG.

Our best standard solar model (model 20) includes helium and heavy element diffusion, has an age of 4.5 Gyr, is

evolved from a homogeneous ZAMS with $X_{\text{init}} = 0.7059$ and $Z_{\text{init}} = 0.020$, and yields a $(Z/X)_{\odot} = 0.0244$ for the present Sun. The flux of neutrinos for ^{37}Cl is 8.35 SNU and for ^{71}Ga is 133 SNU. A detailed listing of the structure of this model may be obtained from the authors.

The second part of the paper is concerned with three classes of nonstandard models which have been proposed in the past as possible solutions of the “solar neutrino problems.” Our aim was to reconsider these nonstandard models in the light of improved stellar physics and to subject them to the test of seismology. Helium and heavy-element diffusion was included in all these models.

Our conclusions are the following:

1. *Low-Z core models.*—The main result is that models with a low- Z core more massive than $0.06 M_{\odot}$ are not compatible with the p -mode small spacings. Compatible models have neutrino flux above 4.25 ^{37}Cl SNU and 116 ^{71}Ga SNU.
2. *Mixed core models.*—Models with mixed cores larger than $0.02 M_{\odot}$ are incompatible with the p -mode data. All models with smaller mixed cores exhibit larger neutrino fluxes than the standard solar model.
3. *Mixed shell models.*—In solar models with a mixed interior region (mixed shell), the effect on the p -mode frequencies depends on how close to the center the mixing takes place. The effect on the p -mode frequencies is minimal for models in which mixing takes place primarily in a region where the run of the ^4He abundance is unaltered by nuclear burning. Closer to the center, mixing between $0.1 M_{\odot}$ and $0.15 M_{\odot}$ is ruled out by the small spacings. If the inner boundary of the mixed region is at $0.20 M_{\odot}$, on the other hand, mixing could extend to $0.4 M_{\odot}$ undetected by the p -mode frequencies. In all these models, the neutrino fluxes are higher than in the standard solar model.

Note that because we have assumed instantaneous mixing in our models, there is no large difference in the calculated ^7Be and ^8B neutrino fluxes, as compared with the standard solar model. Our models thus differ in this context from the model suggested by Cumming & Haxton (1996), in which the mixing within the Sun is taken to be slow. Our calculations show that the model proposed by Cumming & Haxton (1996) is ruled out by seismology, since ^4He is mixed at the same time as ^3He in the deep interior in their model. However, seismology cannot at this point rule out models in which ^3He and other trace elements are slowly mixed in the interior in the region where the ^4He abundance is nearly uniform. In such models, it is possible that the predicted $^7\text{Be}/^8\text{B}$ neutrino flux ratio could be modified without changing noticeably the run of the sound speed in the region.

This work was supported in part by an NSERC grant to D. B. G.

REFERENCES

- Abdurashitov, J. N., et al. 1994, LANL Rep. LA-UR-94-1113
 Alexander, D. R., & Ferguson, J. W. 1994, ApJ, 437, 879
 Anselmann, P., et al. 1994, Phys. Rev. Lett., B327, 377
 Antia, H. M., & Basu, S. 1994, ApJ, 426, 801
 Bahcall, J. N. 1989, Neutrino Astrophysics (Cambridge: Cambridge Univ. Press)
 Bahcall, J. N., Bahcall, N. A., & Ulrich, R. K. 1968, ApJ, 2, 91
 Bahcall, J. N., & Pinsonneault, M. H. 1992, Rev. Mod. Phys., 60, 297
 Bahcall, J. N., Pinsonneault, M. H., & Wasserburg, G. J. 1995, Rev. Mod. Phys., 67, 781
 Balantekin, A. B., & Bahcall, J. N., ed. 1994, Proc. Solar Modeling Workshop, Inst. Nucl. Theory, Univ. Washington, Seattle (New Jersey: World Scientific)
 Chaboyer, B., Demarque, P., Guenther, D. B., & Pinsonneault, M. H. 1995b, ApJ, 446, 435
 Chaboyer, B., Demarque, P., & Pinsonneault, M. H. 1995a, ApJ, 441, 865
 Chaplin, W. J., Elsworth, Y., Howe, R., Isaak, R., McLeod, C. P., Miller, B. A., & New, R. 1996, MNRAS, 280, 1162
 Christensen-Dalsgaard, J. 1986, in Seismology of the Sun and the Distant Stars, ed. D. O. Gough (Dordrecht: Reidel), 23

- Christensen-Dalsgaard, J. 1992, *ApJ*, 385, 354
Christensen-Dalsgaard, J., et al. 1996, *Science*, 272, 1286
Christensen-Dalsgaard, J., & Gough, D. O. 1980, *Nature*, 288, 544
Christensen-Dalsgaard, J., Gough, D. O., & Thompson, M. J. 1991, *ApJ*, 378, 413
Christensen-Dalsgaard, J., Proffitt, C. R., & Thompson, M. J. 1993, *ApJ*, 403, L75
Cox, A. N., Guzik, J. A., & Kidman, R. B. 1988, *ApJ*, 342, 1187
Cumming, A., & Haxton, W. C. 1996, Rep. No. nucl-th/9608045
Däppen, W., & Gough, D. O. 1986, in *NATA ASI Ser. C 169, Seismology of the Sun and the Distant Stars*, ed. D. O. Gough (Dordrecht: Reidel), 275
Davis, R., Jr. 1993, in *Frontiers in Neutrino Astrophysics*, ed. Y. Suzuki & K. Nakamura (Tokyo: Tokyo Universal Acad. Press)
Demarque, P., Guenther, D. B., & Kim, Y.-C. 1997, *ApJ*, 474, 790
Demarque, P., Sarajedini, A., & Guo, X.-J. 1994, *ApJ*, 426, 165
Dilke, F. W. W., & Gough, D. O. 1972, *Nature*, 240, 262
Dinescu, D. I., Demarque, P., Guenther, D. B., & Pinsonneault, M. H. 1995, *AJ*, 109, 2090
Elsworth, Y., Howe, R., Isaak, G. R., McLeod, C. P., & New, R. 1990, *Nature*, 347, 536
Ezer, D., & Cameron, A. G. W. 1968, *ApJ*, 1, L177
———. 1972, *Nature Phys. Sci.*, 240, 180
Grevesse, N., Noels, A., & Sauval, A. J. 1996, in *ASP Conf. Ser. 99, Cosmic Abundances*, ed. S. S. Holt & G. Sonneborn (San Francisco: ASP), 117
Guenther, D. B. 1989, *ApJ*, 339, 1156
———. 1994, *ApJ*, 422, 400
Guenther, D. B., Demarque, P., Kim, Y.-C., & Pinsonneault, M. H. 1992, *ApJ*, 387, 372
Harvey, J. W., et al. 1996, *Science*, 272, 1284
Hata, N., et al. 1994, *Phys. Rev. D*, 49, 3622
Haxton, W. C. 1995, *ARA&A*, 33, 459
Hoyle, F. 1975, *ApJ*, 197, L127
Iglesias, C. A., & Rogers, F. J. 1996, *ApJ*, 464, 943
Krishna Swamy, K. S. 1966, *ApJ*, 145, 174
Prather, M., & Demarque, P. 1974, *ApJ*, 193, 109
Prentice, A. J. R. 1973, *MNRAS*, 163, 331
Raghavan, R. S. 1995, *Science*, 267, 45
Rogers, F. J. 1986, *ApJ*, 310, 723
Rogers, F. J., Swenson, F. J., & Iglesias, C. A. 1996, *ApJ*, 456, 902
Rood, R. T. 1972, *Nature Phys. Sci.*, 240, 178
———. 1978, in *Proc. Informal Conf. Status and Future of Solar Neutrino Research*, ed. G. Friedlander, BNL-50879, 1, 175
Sackmann, I.-J., Boothroyd, A. I., & Fowler, W. A. 1990, *ApJ*, 360, 727
Shaviv, G., & Salpeter, E. E. 1971, *ApJ*, 165, 171
Strom, S. E., Edwards, S., & Skrutskie, M. F. 1993, in *Protostars and Planets*, Vol. 3, ed. E. H. Levy & J. I. Lunine (Tucson: Univ. Arizona Press), 837
Tassoul, M. 1980, *ApJS*, 43, 469
Turck-Chièze, S., Cahen, S., Cassé, M., & Doom, C. 1988, *ApJ*, 335, 415
Ulrich, R. K., & Rhodes, E. J., Jr. 1983, *ApJ*, 265, 551
Ulrich, R. K., & Rood, R. T. 1973, *Nature Phys. Sci.*, 241, 111
Wheeler, J. C. 1979, *ApJ*, 234, 569